Railway Engineering Science
https://doi.org/10.1007/s40534-026-00450-7

Design, modelling, testing and application of hydraulic suspension components for rail vehicles: a state-of-the-art review

Gioele Isacchi[1] · Huailong Shi[2] · Francesco Ripamonti[1] · Jing Zeng[2] · Stefano Bruni[1]

Received: 7 April 2026 / Revised: 14 June 2026 / Accepted: 16 June 2026

Abstract

Rail transport is a safe, efficient and ecological way to meet the growing demand for a more connected and developed society. In the last decades, the development of passenger rail vehicles with improved ride quality and higher commercial speed have been supported by the research and optimization of new suspension components. Hydraulic suspension components (HSCs) represent a significant share of the most recent innovations proposed in this context. This paper provides a state-of-the-art review of the design, modelling, testing and application of HSCs, also discussing the effect of degradation and failure in these components. The paper aims to highlight the most recent advancements in these fields and the emerging trends that will likely be addressed in the near future to further support the development of new rail vehicles.

Keywords Damper · Hybrid simulation · Railway dynamics · Active suspensions · Stability · Curving · Ride quality

1 Introduction

Hydraulic suspension components (HSCs) are widely used in modern rail vehicles and their design deeply affects the vehicle's running behaviour in many respects, including stability, curving behaviour, ride quality and inter-car forces. Therefore, intense research effort has been paid in recent years to optimise the design of conventional passive HSCs, define and assess innovative concepts for non-conventional HSCs including semi-active (SA) and full-active (FA) solutions, and to propose and validate accurate models of these components, which are a critical part of the multibody (MB) models typically used to investigate the running behaviour of rail vehicles.

Passenger vehicles rely on HSCs to dissipate energy considering their superior performance with respect to friction devices [1]. These devices are part of both the primary and secondary suspension stages. Primary HSCs are generally mounted in vertical direction, but research works [2–5] proposed the use of smart HSCs in longitudinal direction to improve curving performance. HSCs also connect the motor system to the bogie frame [6, 7] and to provide energy dissipation in the pantograph system [8, 9]. Articulated vehicles also feature inter-car dampers between adjacent car bodies to suppress the low-frequency modes [10].

The modelling of HSCs is particularly challenging, as these components typically show a nonlinear behaviour, and the output force is dependent on amplitude and frequency of deformation, as well as on the temperature. Moreover, these components include solid parts, made of metallic and elastomeric materials, and fluids, thus requiring a Multiphysics modelling approach which may lead to significant model complexity and computational cost. Alternatively, equivalent models (such as the Maxwell model, see Sect. 3.1) can be established, but need to be carefully calibrated using suitable parameter identification techniques to ensure a satisfactory level of accuracy.

The aim of this paper is to provide a comprehensive review of HSCs in rail vehicles in terms of their use in different parts of the vehicle, their architecture and working principles (Sect. 2), modelling approaches (Sect. 3), testing and experimental characterisation methods (Sect. 4), effect on vehicle dynamics and structural vibration (Sect. 5), specific failure and degradation phenomena (Sect. 6). Moreover, the main emerging and future trends in the use of HSCs in rail vehicles are identified (Sect. 7).

✉ Gioele Isacchi
gioele.isacchi@polimi.it

[1] Dipartimento Di Meccanica, Politecnico Di Milano, 20156 Milan, Italy

[2] State Key Laboratory of Rail Transit Vehicle System, Southwest Jiaotong University, Chengdu 610031, China

2 Hydraulic suspension components in rail vehicles

2.1 Classification based on their implementation inside the vehicle

HSCs can be classified according to their mounting position inside the rail vehicle:

- Primary HSCs: divided into vertical and longitudinal solutions.
- Secondary HSCs: implemented in lateral, vertical and longitudinal (yaw) direction.
- HSCs to connect the traction motor unit to the bogie frame.
- HSCs implemented in pantograph systems.
- Inter-car dampers linking adjacent car bodies along different directions.

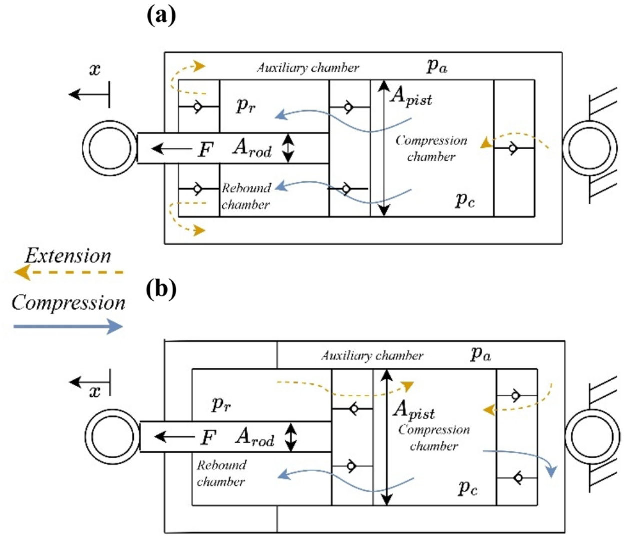

Fig. 1 Synthetic illustration of internal oil flows in extension and rebound strokes of **a** single flow HSC and **b** double flow HSC

2.2 Classification based on their architecture

HSCs for railway applications can also be classified into two main architectures: independent twin-tube components and Hydraulic Interconnected Suspensions (HIS).

2.2.1 Independent twin-tube HSCs

In twin-tube HSCs (also known as double-tube), two concentric tubes are used, and the exterior annulus contains some gas to accommodate the rod displacement volume [11].

Most of the HSCs for railway applications are independent components based on twin-tube design, and feature either single flow (SF) or double flows (DF) layouts. As shown in Fig. 1, both layouts are composed of a rebound chamber, a compression chamber and an auxiliary chamber. While the first two chambers are almost completely filled with oil (with the only exception of minor gas quantities dissolved in the oil), the auxiliary chamber has a relevant amount of gas inside. The SF and DF layouts feature different valve subsystems:

- SF dampers, see Figure 1a, implement valve components designed to allow the oil flowing along a single direction [12–15]. One-way valves (also known as check valves) are introduced in the piston, at the interface between rebound and auxiliary chambers and at the bottom of the compression chamber. When compressed, the piston valves allow the oil to flow from the compression to the rebound chamber, to balance the variation in the chambers' volume. When extended, the piston valves are closed and the oil flows from the rebound to the auxiliary chamber and from the auxiliary to the compression chamber.
- DF dampers, see Figure 1b, do not feature connections between the rebound and auxiliary chambers. The piston and check valves between the compression and auxiliary chambers allow the oil to flow in both directions [12, 16]. Therefore, when the damper is compressed, the oil flows from the compression chamber to the rebound and auxiliary chambers, while when the damper is extended the oil flows in the opposite direction (from rebound and auxiliary chambers to the compression chamber). It is important to note that the configuration of the valves between compression and auxiliary chambers is generally asymmetric: a spool valve is introduced to allow oil flow during the compression phase, while a check valve with a very low dissipation allows the oil flow in the extension phase [17].

According to Fig. 1, considering the piston area A_{pist} and the rod area A_{rod}, the damper force F can be defined as

$$F = p_{\mathrm{c}}A_{\mathrm{pist}} - p_{\mathrm{r}}\left(A_{\mathrm{pist}} - A_{\mathrm{rod}}\right). \tag{1}$$

where p_{c}, p_{r} represent the pressure in the compression and rebound chambers, respectively.

2.2.2 Hydraulic interconnected suspensions

Beside traditional layout, in the last years an innovative architecture was proposed, featuring hydraulic interconnections across difference cylinders. This layout is known as Hydraulic Interconnected Suspension (HIS). HISs are generally introduced in a symmetric layout, such as symmetrically placed secondary vertical dampers [18, 19] or primary vertical dampers [20], or pairs of symmetric yaw dampers installed on the same bogie [21]. The interconnection of two cylinders allows to differentiate the response of the HIS depending on the relative phase between the motion applied to the pistons of the pairs of symmetrical units. This allows, for example, to decouple the response of the HIS to roll and vertical excitation [20].

2.3 Classification based on physical working principles

HSCs can also be classified according to their working principles, as shown in Fig. 2. In particular, the following layouts can be distinguished:

- Passive suspension (PS) components: traditional components characterised by a fixed (non-tuneable) behaviour. Their design sometimes involves trade-offs between contrasting performance aspects such as stability versus ride quality [22–24].
- Smart passive (SP) components: passive suspensions featuring complex internal layouts able to strongly vary their dynamic characteristics according to the operating conditions, without requiring any sensor, controller or power supply. These components are designed to be easily implemented in rail vehicles, directly replacing standard PS components. Examples of SP hydraulic dampers for railway applications based on innovative valves are discussed in [25, 26]. SP hydraulic suspension components based on hydraulic bushings were also proposed [27, 28].
- Semi-Active dampers (SADs): the dynamic characteristics of these suspension elements can be altered by means of an external controller. SADs require the introduction of sensor(s), a control unit and some limited power supply.
- Fully active dampers (FADs): also known as full-active suspension, these devices basically consist of a controlled actuator capable of providing a wide range of input forces. FADs provide superior performance enhancement with respect to SADs and passive HSCs [29], but their use entails the availability of significant power to feed the actuators, leading to larger power supply requirements with respect to SADs.

The variation in the dynamic characteristics of SADs and FADs is achieved by considering different technological solutions:

- Continuous variable damping (CVD): it is based on the introduction of servo-valves able to modify the dissipative behaviour of the component. The simplest implementations feature on/off valves in parallel to the traditional passive valves to adapt the damper performance to the running conditions of the vehicle in a discrete way, as reported for example in [12, 30]. More advanced implementations also require the use of proportional servo-valves able to modify in a continuous way the characteristics of the damper [31–33].

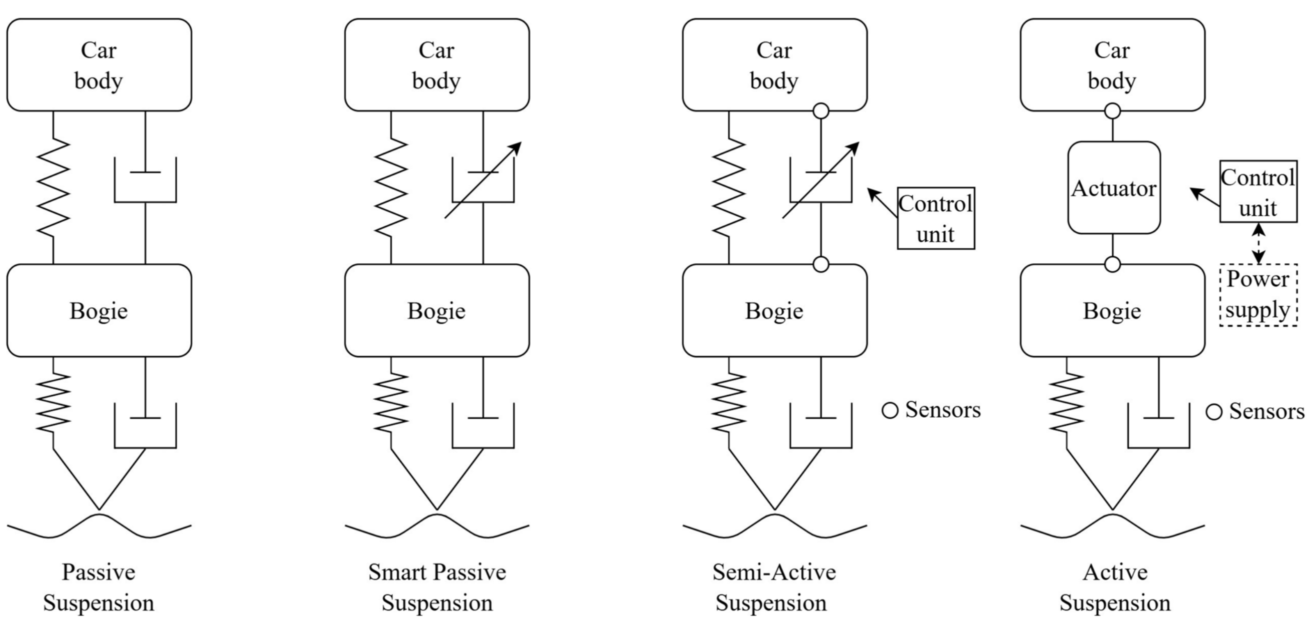

Fig. 2 Comparison of different suspension layouts with increased complexity

- A different SADS concept makes use of magneto-rheological (MR) or electro-rheological (ER) fluids which modify their yield stress depending on either the magnetic field or the electric field to which the fluid is exposed [11], modifying their behaviour from liquid to semi-solid or even plastic [34]. Therefore, variations in the magnetic or electric field allow a smart control of the damper response. Compared to MR dampers, ER dampers are limited by the need of high operating voltage and large power requirement. Moreover, their dynamic performance strongly depend on temperature and liquid contamination [11]. Therefore, this solution has been so far proposed in rail vehicles only for buffers and couplers [35, 36]. In contrast, several applications of the MR technology have been proposed for rail vehicles, mainly in the primary and secondary suspensions [37–42]. A more detailed review of this specific topic can be found in [34].

3 Modelling of hydraulic suspension components in railway engineering

3.1 Lumped parameter models

The simplest methodology to model hydraulic dampers is the use of lumped parameter models (LPMs). LPMs provide acceptable accuracy and require a limited computational effort; therefore, they are widely implemented in MB simulations of rail vehicles [43].

3.1.1 HSC with traditional fluids

The reference approach to model traditional HSCs in railway dynamics is the Maxwell model, composed of a dashpot with an in-series spring. This model is widely implemented in dynamic simulations or suspension parameters optimization [44–47] and a linear version of this model is considered as a reference in EN 13802 standard [48] in the context of damper characterisation. Unfortunately, the Maxwell model offers limited accuracy due to the frequency dependence of its parameters (see also Sect. 4). To increase the accuracy, extended models featuring additional parameters and internal states were proposed, also introducing nonlinear terms in the model of the HSC. Examples of LPMs based on elaborations of the Maxwell model considering nonlinear or bilinear force–velocity and force displacement characteristics can be found in [49–51]. Isacchi et al. [26, 52] and Li et al. [25] modified the nonlinear Maxwell model to introduce a frequency-selective passive valve. Guo et al. [53] proposed an LPM of a yaw damper also considering faulty conditions, based on 7 parameters and 2 nonlinear terms. Isacchi et al. [54] and Ren et al. [55] considered additional mass elements and LPMs based on additional internal states to replicate the dynamics of HSCs. Up to now, limited attention was focussed on the use of the more complex Zener model [52].

3.1.2 HSC with ER and MR fluids

Dedicated LPMs are considered when modelling HSCs with MR fluids. The easiest approach to model these components is to implement a quasi-static force–velocity–current nonlinear map. In railway dynamics, this approach was followed by Jeniš et al. [38, 56] to investigate the behaviour of a SA MR yaw damper, with the aim of improving vehicle stability without altering curving behaviour. Another widely used approach is based on the Bouc–Wen model, presented by Bouc [57] and further extended by Wen [58]. In [40], this approach was used to study SA lateral MR dampers. The Bouc–Wen model features a Kelvin–Voigt sub-model (with parameters k_{BW} and c_{BW}) in parallel to a hysteresis sub-model introducing an internal state variable z. The damper force $F_{\mathrm{MR,BW}}$ is defined as a function of the relative displacement x between the damper edges:

$$F_{\mathrm{MR,BW}} = c_{\mathrm{BW}}\dot{x} + k_{\mathrm{BW}}\left(x - x_0\right) + \alpha_{\mathrm{BW}}z, \tag{2}$$

with the dynamics of the internal state variable being defined by

$$z = -\gamma_{\mathrm{BW}}|\dot{x}|z|z|^{n_{\mathrm{BW}}-1} - \beta_{\mathrm{BW}}\dot{x}|z|^{n} + A_{\mathrm{BW}}\dot{x}, \tag{3}$$

where A_{BW}, β_{BW}, γ_{BW}, and n_{BW} represent the amplitude of the hysteresis loop, its shape, the linearity of its transition section, and the smoothness of the transition section, respectively. The term α_{BW} is related to the current I input in the MR device [40], while x_0 represents the undeformed length of the spring [59]. To improve the accuracy of the Bouc–Wen model, a modified formulation was also proposed [60] and applied in MB simulations of rail vehicles [37, 61, 62]. This approach introduces a further internal state y to extend the accuracy of the Bouc–Wen model in a wider range of excitations [59]. The modified model introduces the spring k_{MBW} and the dashpot c_{MBW}, leading to an overall formulation of the damper force F_{MBW} considering a total of 10 parameters. In [37], this approach was proposed to model an SA MR primary vertical damper, also considering its inertial effect by introducing one additional mass parameter m_{MBW}:

$$F_{\mathrm{MR,BW}} = c_{\mathrm{MBW}}\dot{y} + k_{\mathrm{MBW}}\left(x - x_0\right) + m_{\mathrm{MBW}}\ddot{x}, \tag{4}$$

with

$$\dot{y} = \frac{1}{c_{\mathrm{BW}}+c_{\mathrm{MBW}}}\left(\alpha z + c_{\mathrm{BW}}\dot{x} + k_{\mathrm{BW}}(x - y)\right), \tag{5}$$

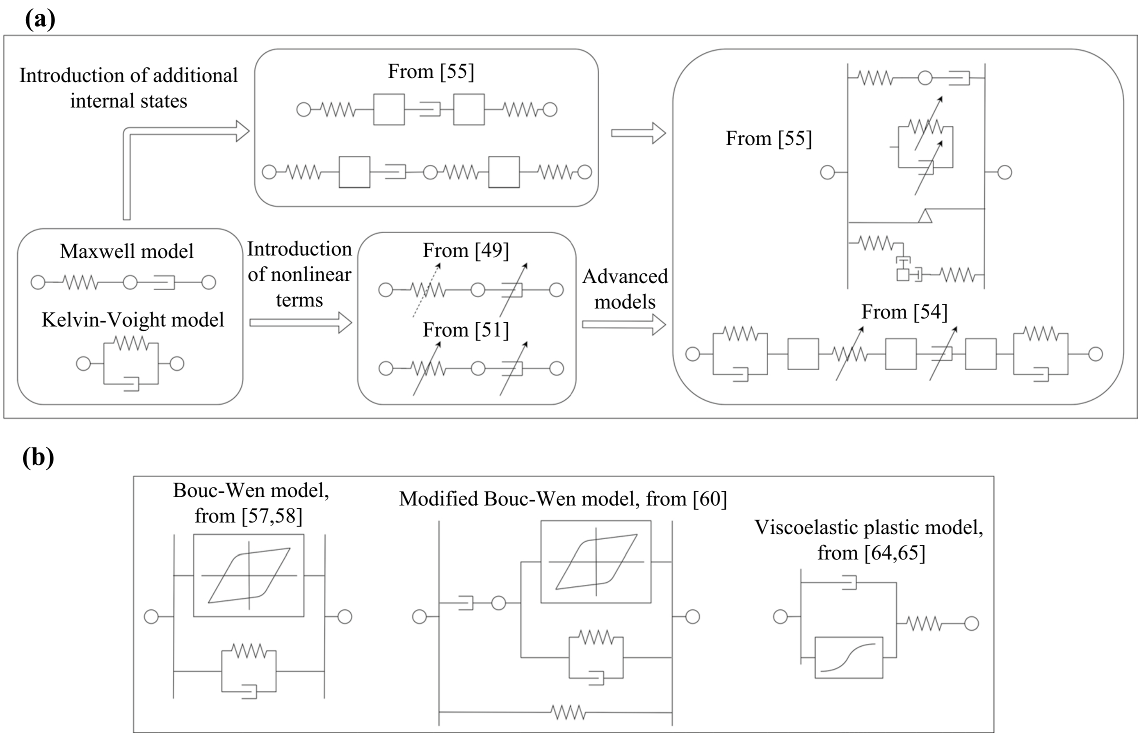

Fig. 3 Overview of the main LPMs considered to model HSCs in the context of MB simulations of rail vehicles: **a** HSCs with conventional fluids; **b** HSCs with MR fluids

$$\dot{z} = -\gamma_{\mathrm{BW}}|\dot{x} - \dot{y}||z|^{n_{\mathrm{BW}}-1}z - \beta_{\mathrm{BW}}(\dot{x} - \dot{y})|z|^{n_{\mathrm{BW}}} + A_{\mathrm{BW}}(\dot{x} - \dot{y}). \tag{6}$$

A further variation was also proposed to investigate the effect of rubber bushings by means of a Kelvin–Voigt sub-model placed in series to the modified Bouc–Wen model [63].

An alternative model based on a viscoelastic-plastic model (VEP) was adopted in [64] to study SA MR lateral damper in rail vehicles. This simplified formulation defines the damper force $F_{\mathrm{MR,VEP}}$ as a function of the current I considering an internal state y [65]:

$$F_{\mathrm{MR,VEP}} = k_{\mathrm{VEP}}(I)(x - y) = c_{\mathrm{VEP}}(I)\dot{y} + f_{\mathrm{c}}(I)\tanh\left[\alpha_{\mathrm{VEP}}(I)\dot{y}\right], \tag{7}$$

where only four current-dependent terms k_{VEP}, c_{VEP}, f_{c}, and α_{VEP} are present, describing the stiffness in the pre-yield region, the damping in the post-yield region, the yield force and the restoring coefficient, respectively.

In Fig. 3, an overview of the most relevant LPMs discussed in this section is reported, distinguishing between models for HSCs with conventional fluids (Fig. 3a) and models for HSCs with MR fluids (Fig. 3b). Readers interested in further exploring the lumped parameters modelling of MR dampers are encouraged to read the dedicated review proposed by Wang and Liao [59] and Bahar et al. [66].

3.2 Physical modelling

Physical models (PMs) of HSCs aim to model the fluid dynamics phenomena taking place inside the components. With respect to LPMs, this approach often provides more accurate results, but requires a higher number of model parameters. In railway applications, commercial software such as AMESim were used to model yaw damper components with either traditional [67] or innovative [68] valve layouts, with the aim of setting up co-simulation with MB models. Nevertheless, most research works propose PM formulations based on in-house-built fluid dynamic models.

In this section, the definition of PMs is presented with reference to the case of twin-tube dampers shown in Fig. 1. PMs usually consider as input the relative displacement (or relative speed) between the damper ends and calculate the force by considering the instantaneous variation of the pressure inside the damper's chambers. The PM aims to define the internal pressures p_{c} and p_{r} as a function of the imposed stroke x with the aim of calculating the force provided by the damper.

Firstly, the mass conservation equation must be formalised for the internal volumes identified from the HSC layout.

 Springer

3.2.1 Continuity equation applied to the internal volumes

PMs are based on the application of the mass conservation equation to the internal chambers of the HSC. In general, oil compressibility plays an important role and cannot be neglected, particularly in the case of large oil volumes [69]. Usually the dependence of oil density on pressure is linearised in the neighbourhood of a reference isothermal condition, introducing the oil's bulk modulus β. In this way, the continuity equation of the i-th chamber (with volume V_i and pressure p_i), considering N_k entering flows $Q_{i,k}$ and N_j exiting flows $Q_{i,j}$, reads [13, 14, 70, 71]

$$\sum_k^{N_k} Q_{i,k} - \sum_j^{N_j} Q_{i,j} = \dot{V}_i + \frac{V_i}{\beta}\dot{p}_i. \tag{8}$$

To consider the effect of air dissolved in the oil, it is suggested [13, 14, 71] to use an effective bulk modulus β_{eff}, accounting for the influence of the pressure p_i and the proportion ε of air entrapped in the oil:

$$\beta_{\text{eff}} = \frac{\beta p_i}{p_i + \varepsilon\beta}. \tag{9}$$

Differently from compression and rebound chambers, the auxiliary chamber has a relevant amount of air inside [15]. Therefore, the air polytropic expression is considered to account for air compressibility. In this case, the oil can be assimilated to an incompressible fluid, due to air being much more compressible. Considering the oil flows $Q_{k,\text{aux}}$ entering the auxiliary chamber, the continuity equation can be obtained, under the assumption of adiabatic condition [71]:

$$\sum_k^{N_k} Q_{k,\text{aux}} = \left[\frac{V_{\text{aux}}}{\beta} + \frac{p_{\text{a0}}^{1/\gamma}}{p_{\text{a}}^{1/\gamma}}\frac{V_{\text{a0}}}{\beta}\left(\frac{\beta}{\gamma p_{\text{a}}} - 1\right)\right]\dot{p}_{\text{a}}, \tag{10}$$

where V_{aux} represents the auxiliary chamber volume, γ indicates the polytropic index, p_{a} the instantaneous pressure in the auxiliary chamber, while V_{a0} and p_{a0} are the pressure and the volume of air in the auxiliary chamber when the damper is fully extended [12–14, 71].

3.2.2 Models of valves and orifices

Hydraulic valves implemented in HSCs feature different layouts. In railway engineering, focussing on the piston component, the most used applications are spool valves and shim-stack valves. Since simple orifices are also present in the piston, the oil flow through the piston is due to the parallel influences of both orifices and valves: the orifices aim to provide the damping force in traditional service condition, while valves introduce a parallel contribution when the pressure difference across the piston exceeds given design thresholds [16].

The oil flow through an orifice Q_{Orif} can be modelled according to the Bernoulli equation [72] starting from the area A_0 and pressure difference Δp_{Orif} across the orifice, and considering the flow coefficient C_{d}:

$$Q_{\text{Orif}} = C_{\text{d}} A_0 \sqrt{\frac{2\Delta p_{\text{Orif}}}{\rho}}. \tag{11}$$

The non-dimensional flow coefficient is usually assumed to take a constant value ranging from 0.62 to 0.81. Gao et al. proposed refined formulations to model the orifice-working stage of HSC for rail vehicles, considering Reynolds number and the length–diameter ratio of the orifice [16], while Wang [73] modelled a yaw damper by considering flow coefficient formulations correlated to the valve radius and opening height.

Besides orifices with constant area, HSCs feature spool damping valves, as illustrated in Fig. 4a. These systems are composed of a spool with cross-drilled holes [11, 16] which is centred in a hood and held in position by means of a helical spring. The spool holes are designed to provide the desired flow area as a function of the spool displacement. Generally, four to six valves are implemented in damper pistons, since spool valves act as one-way valves [13, 14, 16, 71]. In [74], the modelling of oil flows through the piston was based on the implementation of Bernoulli's equation, considering the parallel effects of the spool valves and the orifices. In [13], Huang and Zeng proposed a simplified modelling approach to identify the equivalent nonlinear relationship between oil flow Q and pressure difference Δp across the piston capable to simulate the overall influence of spool valves and orifices in the piston of a SF yaw damper. The equivalent relationship was identified from the force–velocity relationship $\left(F, v_{\text{pist}}\right)$ measured in quasi-static tests, considering F as the average value between rebound and compression strokes. The same approach was also extended for a DF yaw damper [75].

In [14], the oil flow Q_{pv} through a complex damping valve of an SF yaw damper composed of an orifice with area A_0 and three spool valves characterised by different diameters d_1, d_2, and d_3 and preload pressures $p_{k1} < p_{k2} < p_{k3}$ was modelled by considering the parallel oil flows through orifice (Q_{Orif}) and through spool valves ($Q_{\text{spool},i}$):

$$Q_{\text{spool},i} = C_{\text{d}}\frac{\pi d_i^2}{4}\sqrt{\frac{2\left(p_{in} - p_{ki}\right)}{\rho}}, \tag{12}$$

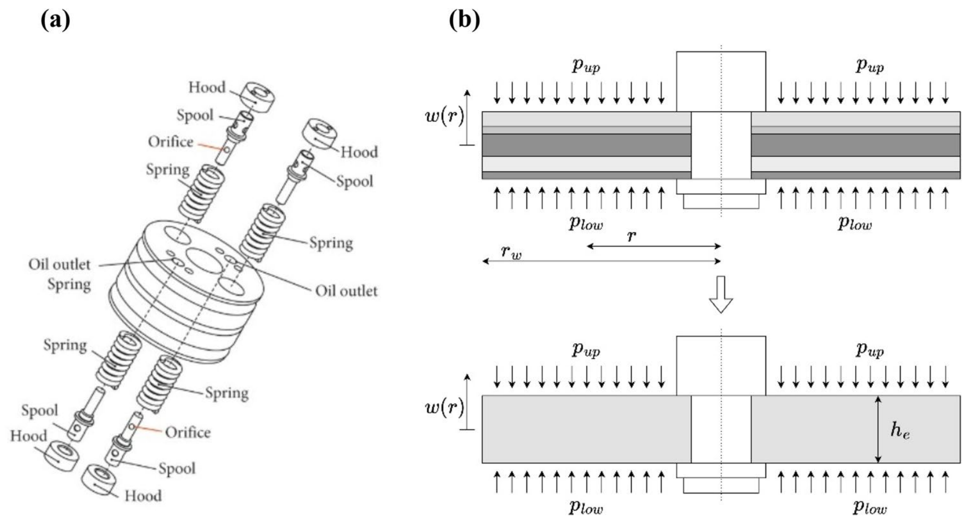

Fig. 4 **a** Overview of the typical layout of a DF damper piston with spool valves, modified from [16] (CC BY). **b** Schematic illustration of a shim-stack valve with multiple discs, and visual representation of the single equivalent disc hypothesis proposed in [76]

$$\begin{cases} Q_{\mathrm{pv}} = C_{\mathrm{d}} A_0 \sqrt{\frac{2(p_{\mathrm{in}} - p_{\mathrm{out}})}{\rho}} & \text{for } (p_{\mathrm{in}} - p_{\mathrm{out}}) < p_{k1} \\ Q_{\mathrm{pv}} = C_{\mathrm{d}} A_0 \sqrt{\frac{2(p_{\mathrm{in}} - p_{\mathrm{out}})}{\rho}} + Q_{\mathrm{spool},1} & \text{for } p_{k1} < (p_{\mathrm{in}} - p_{\mathrm{out}}) < p_{k2} \\ Q_{\mathrm{pv}} = C_{\mathrm{d}} A_0 \sqrt{\frac{2(p_{\mathrm{in}} - p_{\mathrm{out}})}{\rho}} + Q_{\mathrm{spool},1} + Q_{\mathrm{spool},2} & \text{for } p_{k2} < (p_{\mathrm{in}} - p_{\mathrm{out}}) < p_{k3} \\ Q_{\mathrm{pv}} = C_{\mathrm{d}} A_0 \sqrt{\frac{2(p_{\mathrm{in}} - p_{\mathrm{out}})}{\rho}} + Q_{\mathrm{spool},1} + Q_{\mathrm{spool},2} + Q_{\mathrm{spool},3} & \text{for } p_{k3} < (p_{\mathrm{in}} - p_{\mathrm{out}}) < p_{k4} \end{cases}. \tag{13}$$

A similar approach can also be implemented to model a displacement-dependent damping force, in particular when considering HSCs for pantograph systems featuring rod orifices that are progressively opened or closed with the relative motion of the rod [77].

As an alternative to spool valves, railway HSCs can feature shim-stack valves, see Fig. 4b. This valve layout is composed of shim-stacks including several shims with different diameters and thickness [11]. Shim-stacks are placed on orifices, preloaded by means of a nut and designed to achieve a nonlinearly variable flow area according to the pressure difference across them. Shim-stack valves are designed to guarantee the desired damping characteristic and, thanks to the huge number of design variables, this layout has greater flexibility but higher complexity compared to simple spool valves [78].

The oil flow through a shim-stack valve is based on the relative pressure across the valve, $\Delta p = p_{\mathrm{up}} - p_{\mathrm{down}}$, and to its flow area, which is in turn related to its axial deflection w and its external radius r_w. As illustrated in Fig. 4b, by assuming an equivalent thickness h_{e} and a deflection coefficient C_{W} for the shim-stack component [76, 79], the shim-stack valve can be managed as an equivalent disk with homogeneous thickness, allowing to define the axial deflection at the edge of the valve $w(r_{\mathrm{w}})$ as function of the pressure drop Δp:

$$w(r_w) = C_{\mathrm{W}} \frac{\Delta p}{h_{\mathrm{e}}^3}. \tag{14}$$

Therefore, an analytical formulation of the volumetric oil flow Q_{s} across a shim-stack valve is obtained:

$$Q_{\mathrm{s}} = C_{\mathrm{d}} \left(2\pi r_w C_{\mathrm{e}} C_{\mathrm{W}} \frac{\Delta p}{h_{\mathrm{e}}^3}\right) \sqrt{\frac{2\Delta p}{\rho}}, \tag{15}$$

Equation (14) assumes a uniformly distributed pressure on the shim-stack component. Therefore, the correction coefficient C_{e} introduced in Eq. (15) was proposed in [76] to consider the actual pressure distribution. This coefficient is obtained from the minimisation of the differences in the

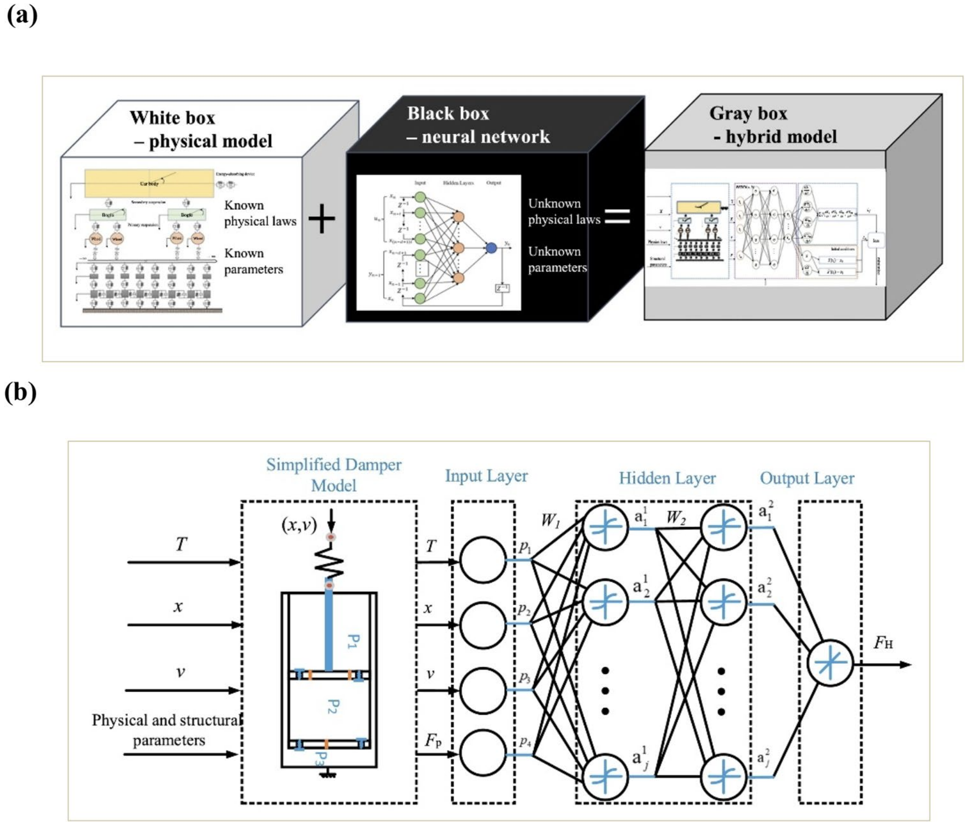

Fig. 5 **a** Typical architecture of a grey box model in the context of railway dynamics, reproduced from [84], with permission from Springer Nature BV. **b** Grey box model of a yaw damper component proposed in [85]

$w(r_w)$ relationship between analytical results and numerical simulations based on finite elements analysis.

3.2.3 Modelling oil leakage

Oil leakages in HSCs take place at the sealing interface between the piston rod and rod guide and between the piston and the cylinder. Kasteel et al. [71] proposed a simplification of the velocity expression of the flow distribution in an annulus [80] to define the oil flow due to leakage in railway HSC. The oil flow $Q_{\text{leak},r\to c}$ across the piston due to leakage can be defined as

$$Q_{\text{leak},r\to c} = \frac{\pi r_l c_l^3}{6\mu L_l}\left[1+\frac{3}{2}\left(\frac{e_l}{c_l}\right)^2\right](p_r - p_c), \tag{16}$$

where r_l is the radius of the piston, c_l is the distance between the piston and the internal cylinder, L_l is the length of the piston, e_l is the eccentricity, and μ the dynamic viscosity of the oil. The oil flow is directed according to the relative pressure difference across the piston. The same formulation can be implemented to define the oil leakage at the interface between the rod and the guide [13].

3.2.4 Modelling of rubber end-mounts

Rubber end-mounts are typically used to connect the HSC to the vehicle. These resilient components have a relevant impact on the high-frequency performance of HSC. Therefore, most PMs consider the effect of the elastic bushings at the two ends of the damper as an equivalent stiffness k_{Bush}, introducing an additional state y to express the relative displacement of the equivalent spring [12, 14]:

$$p_c A_{\text{pist}} - p_r(A_{\text{pist}} - A_{\text{rod}}) = k_{\text{Bush}}(x-y). \tag{17}$$

Other research work introduced equivalent Kelvin–Voigt models to take into account rubber bushings in LPMs [54] and PMs [81].

3.3 Data-driven modelling

Data-driven models (DDMs) correlate a set of inputs with a set of outputs through a series of mathematical formulations. DDMs, also known as black box models, strongly depend on experimental databases of measured inputs and outputs, and their mathematical formulations are based on several parameters that are calibrated in a training phase aiming to minimise the discrepancies between the numerical outputs obtained from the DDM and a partial dataset from the experimental database. After training, the calibrated DDMs are validated and tested using the part of the dataset not considered during the training phase. If correctly calibrated, DDMs are extremely fast models and can provide satisfactory accuracy.

In the context of HSC modelling, a DDM of a secondary SA prototype damper was proposed in [82] to support robustness and failure analyses by means of real-time testing. An ARX model was trained using the MATLAB System Identification Toolbox considering experimental data for damper speeds in the 50–70 mm/s range. The low computational demand of the DDM allowed to test a single prototype by simulating in real-time a virtual twin of the same suspension component mounted on a different location of the vehicle. In [40], a DDM based on artificial neural network (ANN) approach was proposed to identify an inverse model of a SA MR damper. The inverse model was introduced to correlate the reference force identified by the control unit with the correct amount of current to be fed in the MR damper. The same issue was solved in [64] by implementing a more refined DDM based on a nonlinear autoregressive exogenous neural network model (NARX), also featuring a memory ability, and in [83], by proposing a Transfer function—Back Propagation Neural Network inverse model.

DDMs are inherently limited to the damper's working conditions considered in the training dataset. To alleviate this issue, a hybrid approach that merges a DDM with a PM can be considered. In this way, a grey box model able to achieve a good balance between accuracy, physical meaning and computational efforts can be obtained [84]. Figure 5a shows a typical architecture of a grey box model for railway dynamic applications. A DDM (black box) is introduced in series to a PM (white box), with the aim of supporting the accuracy of the PM in presence of unknown physical laws or unknown parameters. According to this principle, a hybrid approach was proposed to model a yaw damper component in [85]. A PM was coupled with an ANN model to further enhance the modelling accuracy, as shown in Fig. 5b. The PM was intended to consider the damper structure (orifices, damping valves, and rubber joints) while the DDM simulated the oil leakage, the internal friction and the amount of air entrapped in the oil. The PM, based on the structural parameters of the damper, took as inputs the temperature, stroke and velocity of the damper, providing a first estimate of the damper force. Then, this preliminary force estimate was then sent to the DDM, together with the original inputs, for further correction before delivering the final force value. The validation of the model showed very good accuracy when tested at frequencies within the training dataset, which was composed of data up to 8 Hz. Moreover, when extending the analysis outside the training dataset (up to 10 Hz), the maximum error was within 8%, showing that hybrid models can provide good extrapolation capability, if supported by accurate PMs.

3.4 High frequency modelling

Most of the research works in the field of HSC for rail vehicles focus their attention on the dynamic performance, limiting the analysis to the 0–20 Hz frequency range. Nevertheless, in recent years, a number of studies have focussed on high-frequency vibration transmission across HSCs to assess their influence on fatigue issues [86, 87] or interior noise [88]. Indeed, suspension components (and traction rods [89]) act as relevant transmission paths for vibration transmission from wheel/rail contact to the single suspended masses (bogies) and double suspended masses (car body).

LPMs were proposed to deal with high-frequency modelling of HSC in railway. In [90], Sañudo et al. proposed to model a primary vertical damper for rail vehicle using a Maxwell model. The stiffness and damping values were obtained by minimising the deviation in dynamic stiffness considering experimental results up to 200 Hz. Nevertheless, a limitation on the compatibility with the testing set-up and the size of the HSC was pointed out. In [47], La Paglia et al. modelled a secondary vertical damper using a LPM based on two internal states, comparing the numerical and experimental trends of the dynamic stiffness up to 30 Hz, in order to perform the optimization of suspension parameters in view of ride quality. A different LPM approach, also considering Kelvin–Voigt formulations for rubber bushings, was proposed in [86] to model primary vertical dampers when studying the vibration insulation of train bogies, targeting a frequency range up to 800 Hz. In this investigation, the damping of the primary vertical damper proved to slightly influence the vibration transmissibility below 300 Hz, leading to less relevant variation with respect to other parameters, such as the stiffness of the axle box rotary arm joint.

In [87, 88], a hybrid modelling approach was proposed to investigate vibration transmission of primary vertical dampers. Firstly, fluid dynamic balance equations were proposed, taking into account the effect of oil compressibility. The flow coefficient was identified from low-frequency tests. Then,

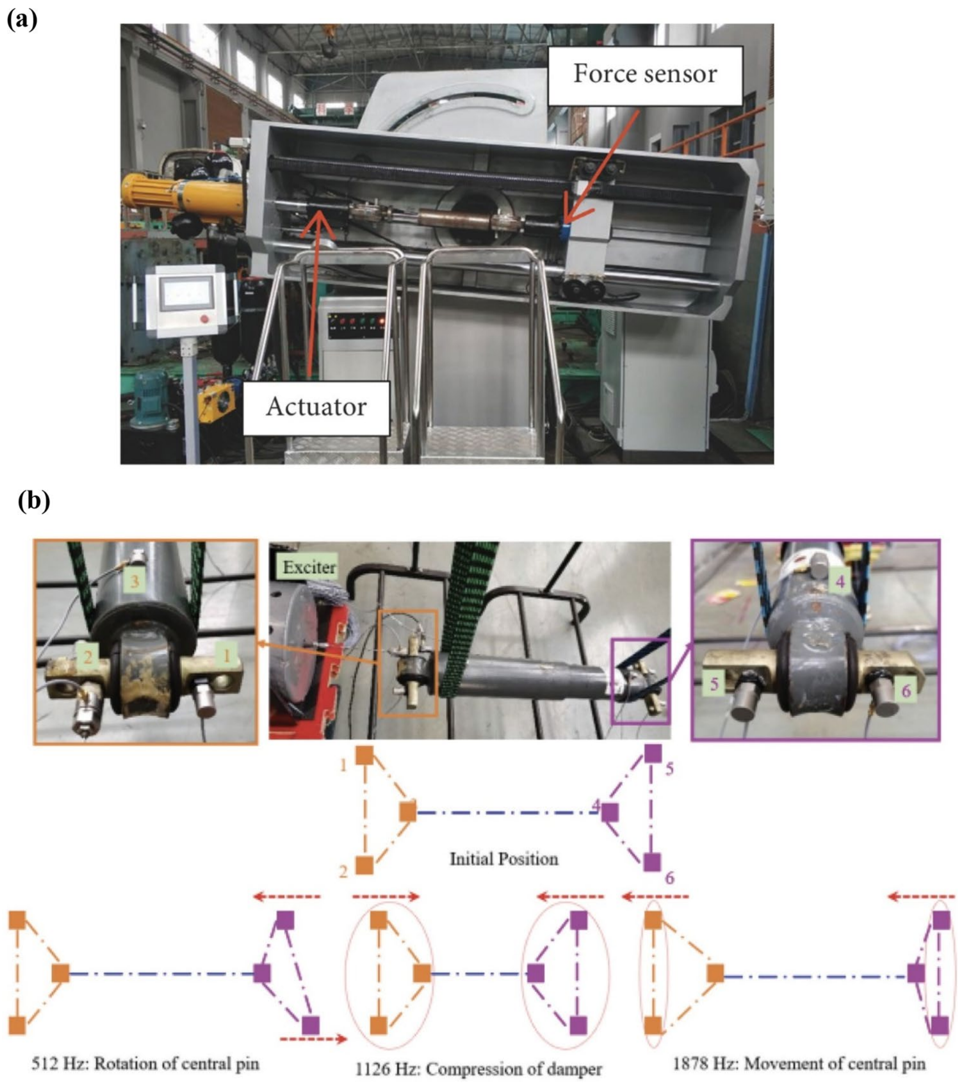

Fig. 6 Testing methodologies for HSCs: **a** characterisation tests of yaw damper components [16] (CC BY); **b** free-free high frequency testing of primary vertical dampers, reproduced from [88]

the damper was divided into three main components (rod, body and pin), and their corresponding mass elements were obtained through free body tests. The rubber bushings were modelled through Kelvin–Voigt model, and the parameters were obtained through high-frequency tests.

4 Testing of hydraulic suspension components in railway engineering

Testing of HSCs for rail vehicles is performed on a regular basis in view of the experimental characterisation of the component, which is required both as part of the type tests for component acceptance and to calibrate mathematical models of the component. This kind of tests is covered in Sect. 4.1. Additionally, advanced and more complex testing methods such as hardware-in-the-loop (HIL) testing and line tests can be performed for special purposes, see Sect. 4.2.

4.1 Characterisation of hydraulic suspension components

According to the EN 13802 standard, characterisation tests of HSCs are conducted by imposing sinusoidal displacements $x(t) = x_0\sin(\omega t)$ on the damper and measuring the force $F(t)$ provided by the device [91]. The standard also proposes typical displacement and velocity values of 1–25 mm and 0.0026–0.5 m/s, respectively. A typical test rig is depicted in Fig. 6a.

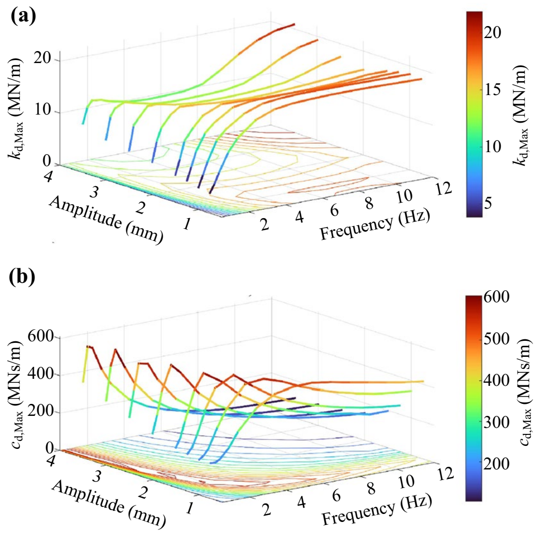

Fig. 7 Comparison of dynamic performance obtained according to EN 13802 from the experimental characterisation of a yaw damper performed at Southwest Jiaotong University, considering different amplitudes and frequencies: **a** dynamic stiffness $k_{d,Max}$; **b** dynamic damping coefficient $c_{d,Max}$

For yaw dampers, two different tests are generally considered:

- Quasi-static tests: sinusoidal cycles with relatively large amplitude (> 10 mm) and low frequencies (< 1 Hz) [13, 26] are imposed to measure the relationship between damper force and piston peak velocity v_0, as illustrated in EN 13802 standard [48].
- Dynamic tests: sinusoidal cycles to study the high frequency response of the damper. In this case, low amplitude (< 2 mm) and higher frequencies (up to 10/15 Hz) values are considered [12, 14, 51].

These tests are consistent with the quasi-static excitation of the yaw dampers in curving and the high-frequency vibration during high-speed straight track running.

Differently from yaw dampers, vertical dampers are generally characterised through sinusoidal cycles combining relatively wide amplitudes with large velocity values. For example, in [37] displacement values up to 16 mm and velocity values up to 0.2 m/s were considered. Due to the influence of vertical dampers on ride quality (see Sects. 5.3.1 and 5.3.2), the testing frequency is generally extended up to 20–30 Hz [37, 47]. Besides sinusoidal cycles at fixed amplitudes, reference displacement signals based on sweeps with fixed velocity values can also be considered to estimate the frequency response of the damper [47].

Lateral dampers are generally tested in similar ways with respect to vertical dampers, combining relevant displacements (for example, 15 mm) with velocity values up to 0.2 m/s [32, 92].

Testing HIS components generally requires additional testing facilities. Indeed, considering the simplest HIS layout, which is based on two cylinders, the testing actuators must be arranged to impose both in-phase excitation and out-of-phase excitation. Eventually, experimental analyses on the single cylinder [93] can be considered as intermediate step.

The experimental characterisation of pantograph dampers can be performed similarly to the other devices. However, it is worth mentioning that pantograph dampers may present larger differences between compression and extension strokes with respect to the other devices. Moreover, pantograph dampers may be designed to increment the damping force when the pantograph reaches the lowered position [8]. Therefore, one of the damper stroke edges would be characterised by much larger damping force: testing operators should be aware of this eventuality and consider to

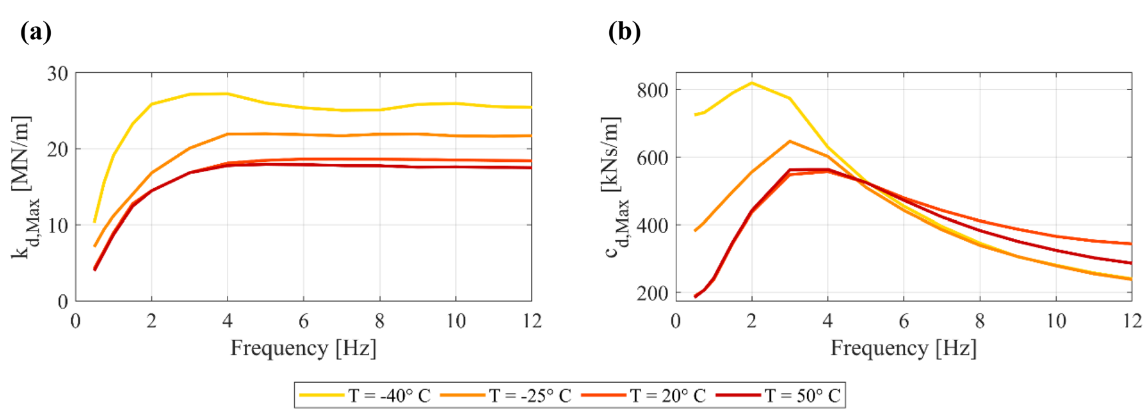

Fig. 8 Effect of environmental temperature on the dynamic performance of a yaw damper excited by sinusoidal cycles of 1 mm amplitude at Southwest Jiaotong University: **a** dynamic stiffness $k_{d,Max}$; **b** dynamic damping coefficient $c_{d,Max}$

characterise these devices in the neighbourhood of different mounting lengths [77], to highlight or prevent the effects of this typical feature of pantograph dampers.

The frequency-dependent behaviour of railway HSCs is usually described by the stiffness and damping coefficients $k_{\mathrm{d,Max}}$ and $c_{\mathrm{d,Max}}$ of an equivalent Maxwell model. The displacement $x(t)$ and force $F(t)$ signals are measured at different frequencies, and the phase shift $\boldsymbol{\Phi}$ between the two signals is obtained by best-fit approximation of the measured signals. The $k_{\mathrm{d,Max}}$ and $c_{\mathrm{d,Max}}$ parameters are then defined as:

$$k_{\mathrm{d,Max}} = \frac{\left(F_{\mathrm{emax},v0}+F_{\mathrm{cmax},v0}\right)}{2x_0}\sqrt{1+\tan^2\boldsymbol{\Phi}}, \tag{18}$$

$$c_{\mathrm{d,Max}} = \frac{k_{\mathrm{d,Max}}}{\omega\tan\boldsymbol{\Phi}}, \tag{19}$$

Considering $F_{\mathrm{emax},v0}$ and $F_{\mathrm{cmax},v0}$ as the maximum force values measured during extension and compression strokes, respectively.

The equivalent Maxwell parameters can also be converted into an equivalent Kelvin–Voigt model consisting in a spring $k_{d_{\mathrm{KV}}}$ and a dashpot $c_{d_{\mathrm{KV}}}$ placed in parallel, as suggested in [94, 95]:

$$k_{d_{\mathrm{KV}}} = \frac{c^2_{d,\mathrm{Max}}k_{\mathrm{d,Max}}\omega^2}{k^2_{\mathrm{d,Max}}+c^2_{\mathrm{d,Max}}\omega^2}, \tag{20}$$

$$c_{d_{\mathrm{KV}}} = \frac{c_{\mathrm{d,Max}}k^2_{\mathrm{d,Max}}}{k^2_{\mathrm{d,Max}}+c^2_{\mathrm{d,Max}}\omega^2}. \tag{21}$$

The measurements of HSC typically show frequency-dependent trends for $k_{\mathrm{d,Max}}$ and $c_{\mathrm{d,Max}}$ that highlights their rheological behaviour. In Fig. 7, the dynamic performance of a yaw damper in good condition ($k_{\mathrm{d,Max}}$ and $c_{\mathrm{d,Max}}$) is illustrated, considering sinusoidal cycles with different combinations of frequency, amplitude and velocity values. Moreover, since the temperature has a relevant effect on the dynamic performance of HSCs, Fig. 8 reports the variation of $k_{\mathrm{d,Max}}$ and $c_{\mathrm{d,Max}}$ at different temperatures. Focussing on the $k_{\mathrm{d,Max}}$ reported in Figs. 7a and 8a, it can be observed that:

- $k_{d,\mathrm{Max}}$ presents a typical increasing trend with the frequency, consistently with previous research works [47, 51, 96]. This trend is almost monotonic at small amplitudes, but at intermediate amplitudes, a decreasing trend can also be observed after 2 Hz.
- $k_{\mathrm{d,Max}}$ varies according to the amplitude of the sinusoidal cycles in different ways. Generally, larger amplitudes lead to a reduction of the dynamic stiffness, in accordance with previous analyses [13]. Nevertheless, it can be observed in Fig. 7a that increasing the amplitude at specific frequencies (such as 8 Hz) could lead to an initial increase in $k_{\mathrm{d,Max}}$ followed by a more complex trend.
- A reduction of temperature introduces a consistent increase in $k_{\mathrm{d,Max}}$. Indeed, an increase in the dynamic stiffness can be observed at every frequency in Fig. 8a, in accordance with previous analyses [97].

  Focussing on the $c_{\mathrm{d,Max}}$ reported in Figs. 7b and 8b, the following observations are highlighted:
- When the frequency increases, a decrease in $c_{\mathrm{d,Max}}$ is generally observed [13, 96], even if the trend of $c_{\mathrm{d,Max}}$ might present an initial increasing trend for a limited frequency interval.
- With the increase in amplitude, the dynamic damping $c_{\mathrm{d,Max}}$ decreases in a more prominent and consistent way with respect to $k_{\mathrm{d,Max}}$. This phenomenon is in accordance with previous investigations [13].
- The reduction of temperature leads to an increase in the dynamic damping at low frequencies, and to a decrease in the same performance index at high frequencies.

4.1.1 Area method

Besides the procedure described in EN 13802 standard, the equivalent parameters $k_{\mathrm{d,Max}}$ and $c_{\mathrm{d,Max}}$ can also be identified according to the area method [51, 91, 96]. The energy dissipated by the HSC in a cycle is represented by the cycle area A in the force versus displacement plot:

$$A = \int_o^s x(t)\mathrm{d}F(t) = c_{\mathrm{d,Max}}x_0^2\omega\pi, \tag{22}$$

where $x(t)$ indicates the relative displacement of the damper piston. After obtaining the cycle area A, it is possible to identify the parameters of the Maxwell model according to [96]:

$$c_{\mathrm{d,Max}} = \frac{A}{\omega\pi\left(x_0\sin\boldsymbol{\Phi}\right)^2}, \tag{23}$$

$$k_{\mathrm{d,Max}} = c_{\mathrm{d,Max}}\tan\boldsymbol{\Phi}. \tag{24}$$

The discrepancies between the two methods can vary up to 15.8% for bidirectional flows HSC [51, 96], highlighting the higher sensitivity of the area method to the sampling frequency of data acquisition systems with respect to the method proposed in EN 13802.

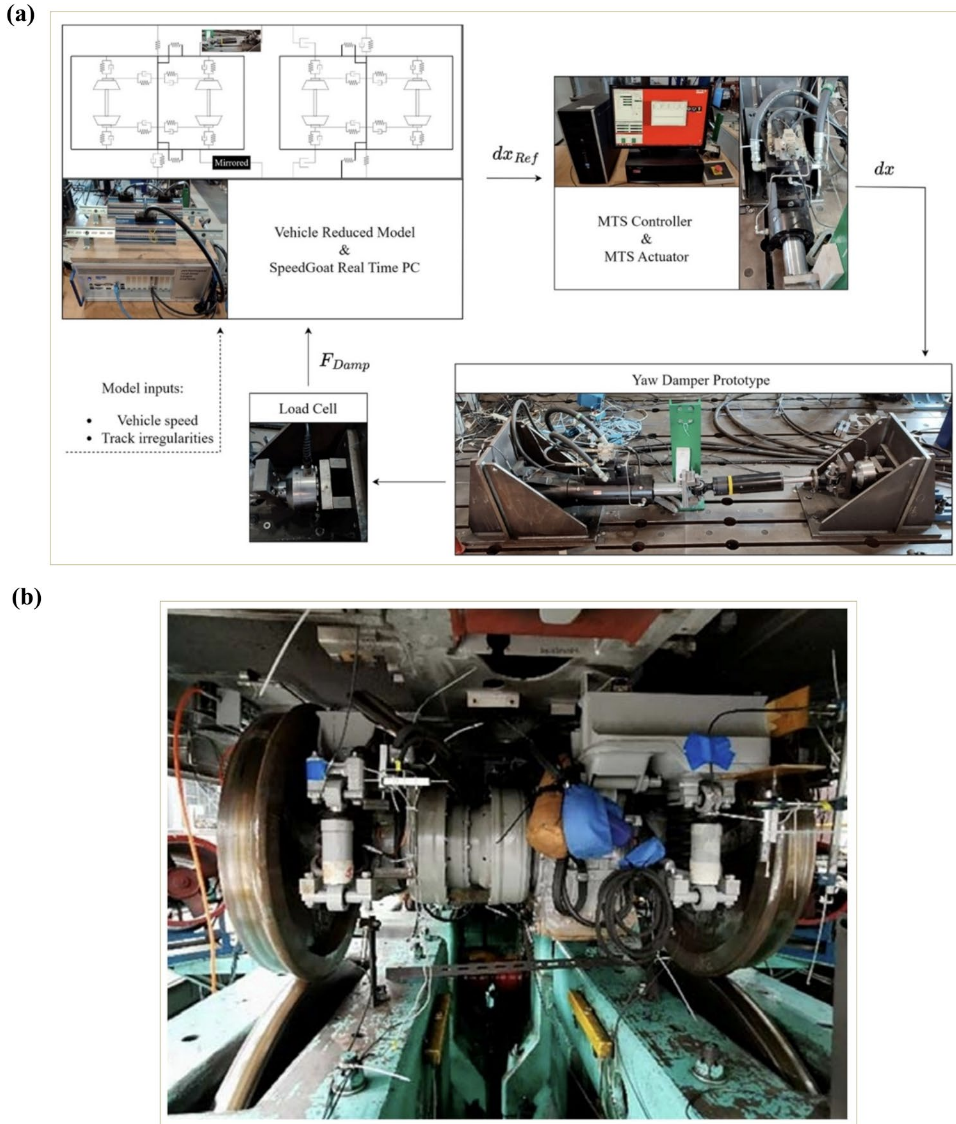

Fig. 9 Testing methodologies for HSCs: **a** hardware-in-the-loop methodology applied to yaw dampers [106], © Taylor and Francis, with permission; **b** roller rig testing of secondary HSC [92]

Frequency domain testing in free–free condition was also proposed as a robust method to quantify the low-frequency dynamic performance of HSCs [96], introducing frequency-domain expressions of the parameters of an equivalent Maxwell model. This approach was also considered at higher frequency ranges (up to 170 Hz) [90].

4.1.2 Tests in free-free condition

A methodology to identify model parameters reproducing the measured free–free dynamics of HSCs was also proposed in [87]. A primary vertical damper was suspended with ropes to simulate free–free condition, and accelerometers were used to measure the response of different components of the HSCs, as shown in Fig. 6b. An electromagnetic shaker was used to imposed high-frequency low-amplitude excitations, and the frequency response functions were obtained to identify the resonances of the damper system. This methodology was also used in combination with traditional quasi-static tests to identify the dissipative response of similar dampers [88].

4.2 Advanced testing of hydraulic suspension components

4.2.1 Hardware-in-the-loop (HIL) testing

Characterisation tests of suspension components are widely implemented to validate numerical models of the systems simulating sinusoidal cycles [13, 14, 51, 73] or realistic scenarios [54, 85]. Generally, after this preliminary calibration, the suspension models are implemented in vehicle models to study their influence on the vehicle dynamics [26, 51, 98–100]. Nevertheless, this methodology is still inevitably affected by the errors between the simulated and the actual response of the HSC.

To experimentally assess physical prototypes, Hardware-In-the-Loop (HIL) methodology has been widely used in many fields of railway dynamics, analysing pantograph–catenary interaction [101–103], trainset longitudinal dynamics [104, 105] and in particular to assist the development of suspension components [31, 37, 106–108]. This methodology, also known as real-time hybrid simulation (RTHS) [109], features a virtual domain and a physical domain. In the virtual domain, a numerical model of a rail vehicle system is integrated in real-time to obtain a reference stroke signal to be imposed on the suspension prototype under analysis. The physical domain consists of a test rig to host suspension prototype(s) and to test them by imposing displacement excitation defined by the vehicle model implemented in the virtual domain [110], which also considers the actual response provided by the prototype(s) and measured on the test rig. Therefore, HIL has the following advantages with respect to traditional HSC characterisation tests [106]:

- HSC can be tested by imposing working conditions which are very close to real operating scenarios.
- The influence of the HSC under analysis on the vehicle dynamic performances can be quantified by assessing the behaviour of the virtual model run during the tests. Indeed, the estimation of the excitation signal obtained from the virtual vehicle model is also a function of the measured response of the prototype(s).

HIL testing of primary and secondary vertical HSCs was proposed in the last years. SA solutions for secondary vertical dampers to improve ride quality were tested through HIL methodology. This methodology allowed to compare skyhook (SH), linear quadratic regulator (LQR) and maximum power point tracking (MPPT) control logics [31] by easily performing several tests. Similarly, HIL supported the robustness and failure analysis [82] of a secondary SA vertical damper with Sliding Mode Control (SMC). The use of HIL allowed to test several working conditions to precisely quantify the capability of the SA damper to deal with unexpected failures or vehicle parameters' variation.

Focussing on primary vertical dampers, HIL supported the application of SA MR components to mitigate the car body bending vibration, supporting the comparison of different control logics [37]. The research on ride quality improvements also focussed on the proposal of innovative lateral HSCs that were assessed through HIL testing, focussing on the proposal of new control logics [107, 111, 112] to mitigate the lateral car body acceleration with SA MR dampers.

HIL testing was also proposed for yaw dampers components (see Fig. 9a), introducing virtual models of the rail vehicle able to simulate bogie hunting behaviour, proposing comparison with MB simulation results [106] or dedicated compensation approaches to minimise the difference between reference and imposed excitations [109]. The wheel–rail contact model introduced in the virtual vehicle models is fundamental in the assessment of vehicle stability. In HIL applications, the normal contact problem is generally simplified, while the tangential contact problem is based on the Shen–Hedrick–Elkins approach [113] considering nonlinear contact geometries, a good compromise between modelling accuracy and computational efficiency.

4.2.2 Full vehicle testing: roller rig tests and line tests

Roller rigs are advanced test facilities that can test rail vehicles (or subsystems of rail vehicles) by simulating running condition. Roller rigs allow to study the interaction between wheels and rails [114]. Full-scale roller rigs can test real vehicles to validate the vehicle design, validate MB models or support the development of innovative suspensions. In [32, 92], roller rig tests were proposed to validate the behaviour of an SA lateral damper, assessing its capability to improve lateral ride quality up to 385 km/h (see Fig. 9b). Similarly, roller rig tests allowed to support the proposal of innovative yaw dampers designed to alleviate the trade-off between car body and bogie hunting [115]. Field tests are one of the most demanding experimental activity in the field of railway engineering; therefore, they are rarely proposed to test new suspension components. Field tests with vehicle speed up to 160 km/h were proposed in [32, 92] to study SA lateral dampers, and FAD vertical HSCs were implemented on a two cars 250 Regina vehicle to measure the improvements in ride quality during field tests [116, 117]. Similar tests were proposed in [118], where the correlation between yaw damper, inter-car damper characteristics and mounting layouts was assessed by means of field tests on a high-speed vehicle. The Railway Technical Research Institute (RTRI) also implemented field tests to verify active primary vertical dampers and air springs, as reported in [119], resulting in a 50% and 20% reduction in the peak of the car body's vertical acceleration power spectral density (PSD) for the bending mode and rigid body mode, respectively.

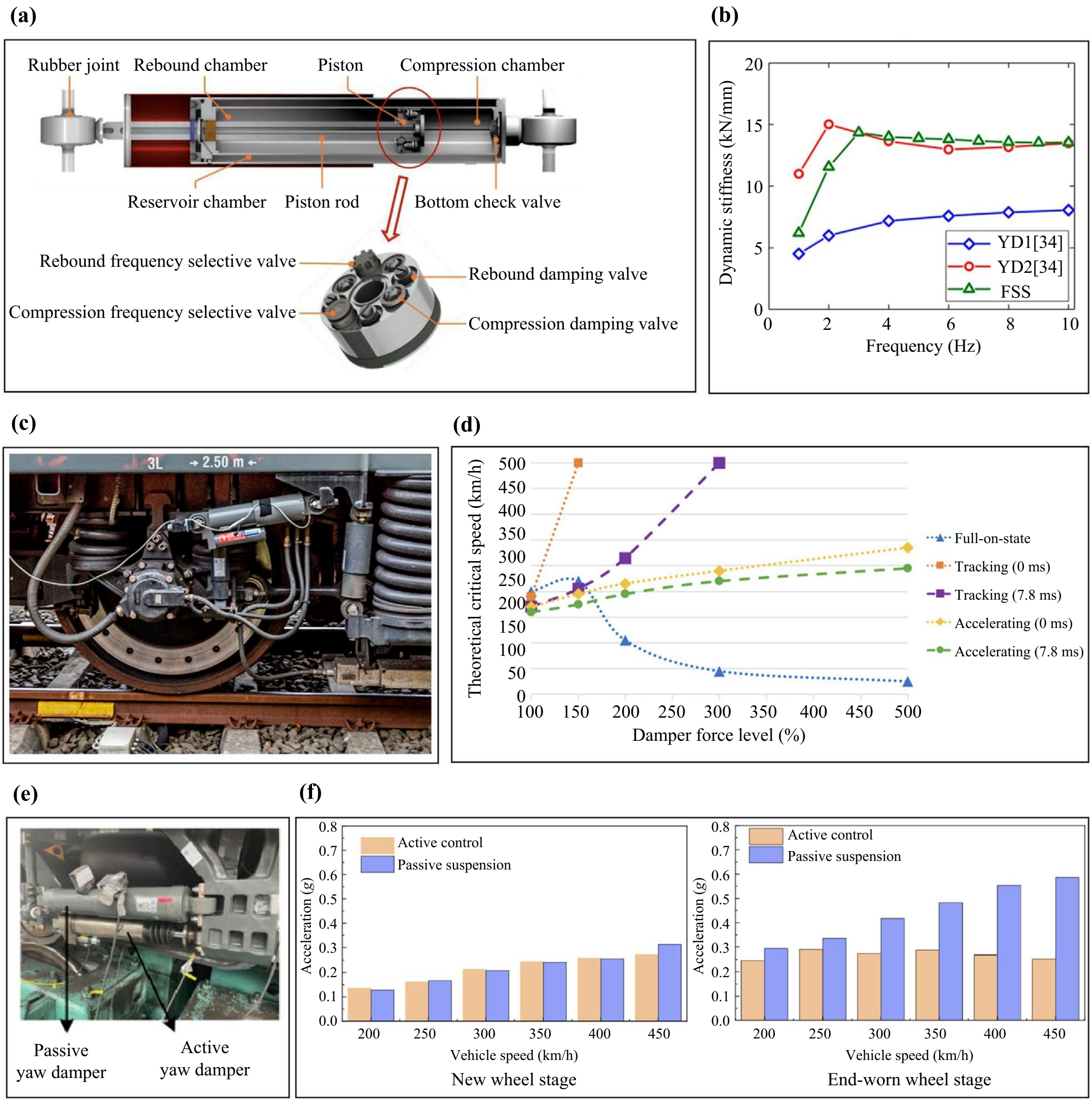

Fig. 10 Relevant yaw dampers applications from recent years: **a** schematization of a SP Frequency Selective Stiffness (FSS) yaw damper; **b** comparison of its dynamic stiffness with traditional dampers (YD1, YD2), measured at 2 mm amplitude, reproduced from [50]; **c** prototype of yaw SAD; **d** simulation of the effect of different control logics and time constant values (t_{63}) on the vehicle critical speed, from [38]; **e** yaw FAD tested on the roller rig facility at Southwest Jiaotong University, and **f** its influence on the maximum bogie frame lateral acceleration at new and end-worn wheel stages (measurements), adapted from [134]

5 Influence of hydraulic suspension components on vehicle dynamics

Rail vehicles feature multiple HSCs in primary and secondary suspension stages. These components affect in many diverse ways the vehicle's dynamic performance. In this section, the effect of HSCs on vehicle stability, curving performance, ride quality, and high frequency structural vibrations is discussed.

5.1 Vehicle stability

The suspension layout has a crucial influence on vehicle stability. Different unstable behaviours have been observed in rail vehicles, which can be categorised as "bogie hunting" and "car body hunting". In this regard, previous studies correlated the occurrence of bogie hunting to wheel–rail geometry with high equivalent conicity [45, 120–123]. In contrast, multiple evidences correlate the occurrence of car body hunting to wheel–rail geometry with low conicity [94, 121, 122, 124, 125]. This latter unstable motion is characterised by a large amplitude low-frequency lateral vibration of the car body and has a detrimental effect on ride quality and running safety due to the discontinuous occurrence of flange contact, even on a straight track. It is important to notice that car body hunting could be more prominent at intermediate speed [46, 126] rather than at high speed, leading to additional challenges in the definition of a vehicle layout able to guarantee stability in the overall range of operating conditions.

5.1.1 Yaw damper's influence on vehicle stability

Linear stability investigations were firstly proposed to provide a panoramic view of the influence of yaw damper components, using Maxwell or Kelvin–Voigt models (see Sect. 3.1). Huang et al. [94] correlated the occurrence of car body hunting with large stiffness and damping parameters of the Maxwell model, denoted hereafter as $k_{d,Max}$ and $c_{d,Max}$, respectively. Sun et al. [124] and Park [125] confirmed this correlation, also identifying the necessity of a minimum value of $k_{\mathrm{d,Max}}$ to prevent the vehicle from showing bogie hunting in case of worn-out wheels. Zhang et al. [127] suggested the existence of an optimal $c_{\mathrm{d,Max}}$ value to limit lateral vibration of high-speed rail vehicles. This trade-off affecting yaw damper parameters has been extensively studied by independently [45] or simultaneously [46] varying the suspension parameters $k_{\mathrm{d,Max}}$ and $c_{\mathrm{d,Max}}$.

Further analyses focussed on the effect of the nonlinear force–velocity curve of the yaw dampers on car body hunting [128] by modelling the component according to a bilinear function described by force and velocity values of the unload point, suggesting the necessity to avoid force unloading. Research also focussed on the optimization of the mounting layout of yaw damper to prevent car body hunting: Jeon et al. [118] modified the layout to prevent unstable yaw torque when the bogie has a lateral velocity, while Huang et al. [129] considered both car body and bogie hunting, demonstrating that a mutual optimization of yaw damper mounting layout and lateral installation angle provides a general improvement of vehicle stability. Nonlinear analyses based on the effect of yaw dampers on the bifurcation behaviour of rail vehicles were also proposed [130, 131], often focussing on bogie hunting.

A notable exception with respect to traditional yaw dampers' layout was studied in [21]: a longitudinal HIS architecture was proposed, taking advantage of its selective response to bogie yaw motion. This application, although highly innovative, achieved modest improvements in terms of low frequency and high frequency hunting.

The trade-off between low and high dynamic stiffness of the yaw damper has been a key topic in the last decade. In order to alleviate this trade-off, HSCs manufacturers proposed SP solutions with specific passive valves introducing pronounced frequency dependent behaviour. Frequency Selective Damping valves were introduced to avoid car body or bogie hunting motions [25]. Similarly, Frequency Selective Stiffness dampers (Fig. 10a) were studied, and good results were obtained in numerical simulations [50] and experimental tests [115], thanks to the variable dynamic stiffness provided by this solution (see Fig. 10b). Zhang et al. [132] proposed an eddy current yaw damper to satisfy the requirements in terms of dynamic stiffness when dealing with car body and bogie hunting, studying its effectiveness with linear analyses.

Researchers also investigated SADs to overcome the limitations affecting passive HSCs. Huang and Zeng [12] proposed a SAD featuring an additional selector valve to vary the yaw dampers' dynamic stiffness, preventing both car body and bogie hunting. Wang et al. [33] studied a SAD prototype to suppress bogie lateral vibration, focussing on high conicity conditions and comparing the effectiveness of MPPT and SH control logics. Jeniš et al. [38] also proposed a SAD (shown in Fig. 10c) to improve vehicle stability, considering both low and high equivalent conicity conditions (Fig. 10d), and comparing a "tracking" control algorithm and a modified Groundhook control.

FADs in longitudinal directions are generally introduced to improve steering performance of rail vehicles, as will be described in Sect. 5.2.2. Nevertheless, some examples were also proposed to improve vehicle stability. Linear [45] and nonlinear [126] numerical investigations showed that active yaw dampers can effectively reduce car body and bogie hunting phenomena. Mao et al. [133] numerically investigated stiffness and damping control of active yaw dampers for high conicity conditions, conducting roller rig tests of active solutions [134], as shown in Fig. 10e, f. In [135], a FAD application based on a Electro-Hydrostatic Actuator (EHA) was numerically assessed showing improvements in bogie stability.

5.1.2 Lateral damper's influence on vehicle stability

Various studies were conducted about the effect of lateral dampers on vehicle stability. In [124], the secondary lateral damper showed limited influence on hunting frequency and modal damping, in accordance with [122]. Zhou et al. [136], Park [125], and Shi et al. [45] confirmed this circumstance, highlighting at the same time a relevant influence of secondary lateral damping on car body modes.

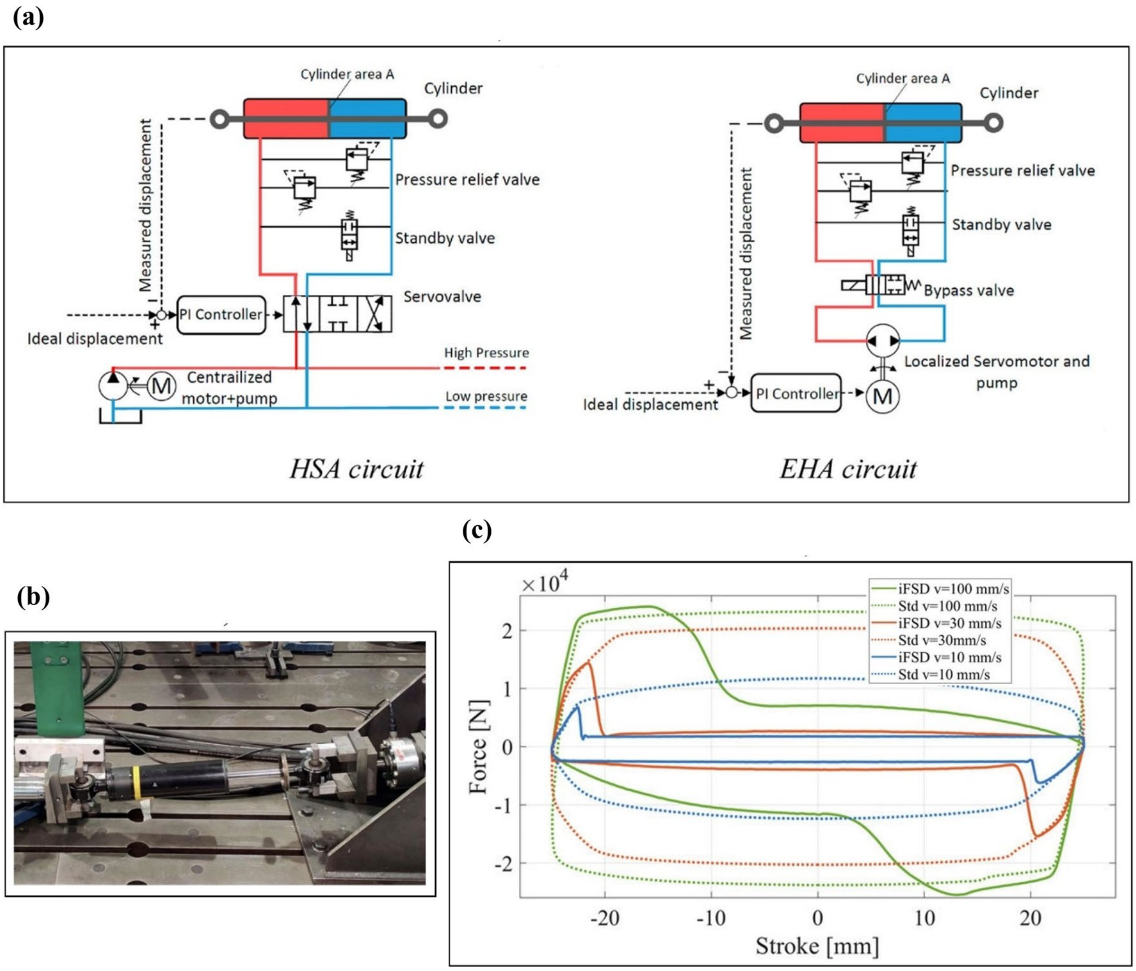

Fig. 11 Applications of innovative HSCs for curving improvement: **a** Comparison of the HSA and EHA layouts from [155]; **b** SP prototype (iFSD) proposed in [26] to reduce bogie steering resistance in comparison with a traditional yaw dampers (Std); **c** comparison of the damping force in low frequency high amplitude characterisation cycles (25 mm), adapted from [26]

Most of the applications of secondary lateral HSCs were focussed on the improvement of low-frequency car body lateral dynamics. Due to their influence on ride quality, these applications will be discussed in Sect. 5.3. Nevertheless, SADs in lateral direction may introduce a slightly detrimental effect on bogie stability [107, 111], even if the car body low-frequency vibration is suppressed. To avoid this issue, SADs based on a self-regulation mixed linear continuous skyhook and groundhook control were proposed [137].

FA and SA layouts for lateral HSCs were numerically investigated in [138] with the aim of suppressing car body hunting, comparing SH damping and stiffness control and on–off control.

5.1.3 Influence of motor HSCs on vehicle stability

The investigation on the influence of motor connection on the bogie stability proposed by Alfi et al. [7] suggested the possibility of tuning the motor resonant frequency f_{mot} and the damping factor ξ_{mot} to increase the critical speed of motor bogies. Subsequently, the tuning of motor HSCs to suppress bogie hunting became a relevant topic in railway research. Huang et al. [139] analysed the motor connection, highlighting a relevant influence of vehicle layout and wheel–rail contact conditions on its optimal tuning. Other works focussed on the influence of motor connections on nonlinear stability [140], considering the effect of nonlinear force–deformation relationship of the motor suspension on the bifurcation behaviour of the vehicle [6]. In the context of global optimization of suspension parameters, Chen et al. [44] also considered motor HSCs, and suggested to calibrate their parameters f_{mot} and ξ_{mot} after identifying the optimal layout of lateral and longitudinal HSCs. Wei et al. [141] extended the motor suspension parameters optimization also considering the effect of motor vibration on the generation of dynamic stresses on the motor hanger component. An unconventional architecture based on bio-inspired design was also proposed in [142] to achieve a nonlinear damping of the motor connections to increase the damping in motor resonance condition, limiting at the same time the damping at higher frequency.

SAD and FAD were also proposed for motor application. Yao et al. [143] investigated different lateral control strategies for the bogie frame, also considering a motor SAD. In [144], a linear actuator was introduced in parallel to the traditional motor connections to obtain an adaptive dynamic vibration absorber to optimise the stability at different wheel–rail conditions: in this way, f_{mot} could be increased for larger conicity thanks to an auto-tuning system monitoring the arising of dominant frequency contributions in the bogie lateral acceleration. The effect of time delay in an active HSCs for motor connection was also explored in [145].

5.1.4 Influence of inter-car HSCs

A pioneering study on the use of inter-car dampers was conducted by Fujimoto and Miyamoto [146], suggesting that these devices could be introduced in rail vehicles to prevent excessive yaw vibration of tail cars in tunnels or during train crossing. The same technology was considered in [118], in regard of longitudinal inter-car dampers introduced in Korea to mitigate the car body swaying of a HEMU-430X train. An extensive analysis was carried out by Wang et al. [147, 148], where lateral inter-car dampers were introduced in transversal direction (acting on the coupler system) to mitigate lateral car body vibration, with smaller influence on the bifurcation behaviour. Using a multi-car MB model, the increase in the damping coefficient of longitudinal inter-car dampers was correlated in [149] with an improvement in vehicle stability (bifurcation behaviour of the first wheelset), considering HSCs mounted in the low or in the upper side of the car bodies' interfaces.

5.2 Curving performance

The trade-off between curving and stability performance have been discussed in the last two centuries, especially with the introduction of bogie systems [150]. To overcome this limitation, primary and secondary HSCs were proposed. This section focuses on the design of HSCs for steering purposes. Readers interested in mechatronic suspensions and active steering topics are referred to previous review papers analysing in detail various control logics and methodologies [151, 152].

5.2.1 Primary suspension stage

Several FA applications were proposed at the primary suspension stage to improve the curving performance of rail vehicles [152]. In [153], the design of an active steering mechanism featuring a single actuator per wheelset was illustrated, focussing on the requirements in terms of actuator moving range. A reduction of creepages and creep forces was observed in numerical simulations and tests on a 1/5-scale model. A simpler layout was proposed in [154], where a single actuator was introduced in every bogie, thanks to a rod and linkages system. In this application, a dedicated hydraulic circuit with improved fail-safe capabilities was also illustrated. In [155], hydraulic servo actuator (HSA) and EHA technologies (compared in Fig. 11a) were considered for steering bogie application, and several configurations were studied and compared in terms of curving performance improvement and fault-tolerant capabilities, proposing co-simulation of MB vehicle model and PMs of the various configurations. In [156], a similar methodology was proposed to numerically evaluate an EHA steering bogie focussing on wheel wear while also confirming the absence of detrimental effects on ride quality.

5.2.2 Secondary suspension stage

The yaw damper is the most influential secondary HSC for curving performance. Theoretical [95] and experimental [157] studies quantified the increase in bogie steering resistance during transient curves due to the presence of yaw dampers. To alleviate this detrimental effect, SP HSCs were successfully introduced. Isacchi et al. [26] and Deng et al. [68] investigated a frequency-dependent SP yaw damper to mitigate the steering resistance in transient curved tracks (see Fig. 11b), studying its effectiveness by means of MB simulations. This device was designed to reduce the damping force for large-amplitude low-frequency excitations, as shown in Fig. 11c. A SP yaw damper with a distinctive position-dependent damping force [100] was proposed and optimised to reduce the track shifting force at different curve radii. Besides the introduction of innovative layouts, in [158] it was observed that the mounting position and installation angle of the yaw dampers affect the maximum wheel wear depth (while less significant effects were observed in stability performance).

Secondary Yaw Control (SYC), i.e. the control of the yaw torque imposed on the bogie from the car body [151], can be achieved through yaw SADs or FADs to increase curving performance. SADs based on CVD [30] and MR [56] technologies were proposed, highlighting the possibility of varying the yaw dampers' characteristics to mitigate the deterioration of curving performance in sharp curves. The RTRI also tested a FA application based on EHA layout

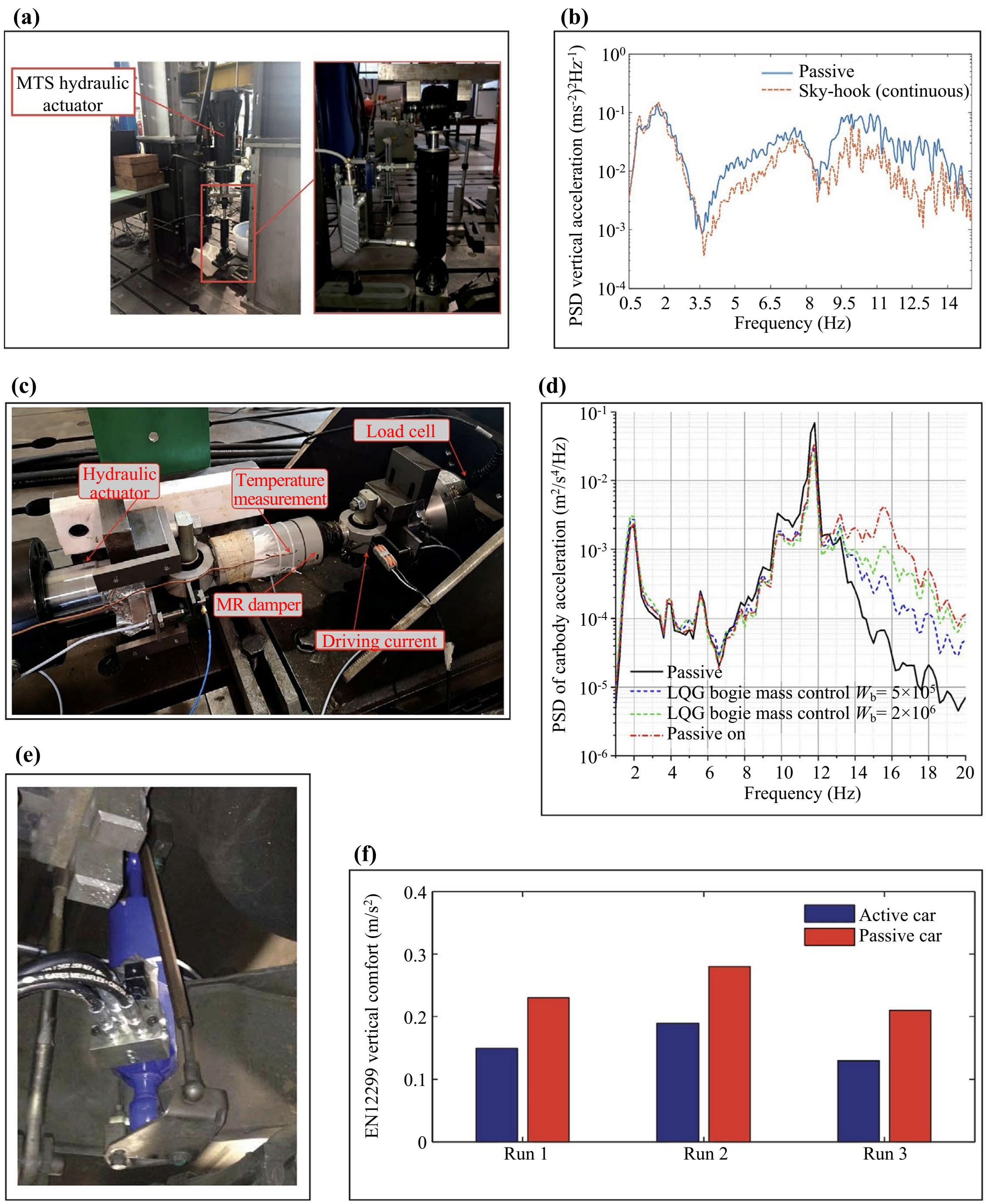

Fig. 12 Application of vertical SAD and FAD for ride quality improvement: **a** secondary CVD SAD and **b** its influence on the PSD of the car body vertical acceleration obtained from HIL testing with the most promising control logic (SH), adapted from [31]; **c** primary vertical MR SAD to suppress car body bending vibration and **d** its effect on the PSD of the car body vertical acceleration with the most effective logic (LQG) during HIL tests, adapted from [37]; **e** secondary vertical SAD and **f** ride quality improvements measured from field tests along three different lines, reproduced from [116]

through field tests [159], evaluating its effect on reducing the track shifting force.

5.3 Ride quality

Ride quality is correlated to the capability of isolating the vehicle body from track irregularities [152]. The assessment of ride quality is strongly related to the sensitivity of human beings to vibration, which is different in vertical and transversal directions [160]. In railway dynamics, three main phenomena can be correlated with passengers' discomfort:

- the transmission of vertical vibration from wheel–rail contact to the car body;
- the perception of non-compensated lateral acceleration and jerk during curve negotiation;
- the low-frequency lateral acceleration due to car body hunting.

Due to its strong link with vehicle stability, the influence of HSCs on the last phenomenon was previously discussed in Sect. 5.1. Therefore, this section focuses on the influence of HSCs on the other two phenomena to provide a complete overview on ride quality issues.

5.3.1 Secondary vertical dampers

The performance of secondary vertical dampers influences the car body vertical acceleration. Wang et. al [76] introduced parameters variation in a shim-stack PM of a secondary vertical damper. Then, co-simulations of the PM with a MB vehicle model identified as the most influent parameters for the vertical car body acceleration the in-series stiffness of the rubber bushings and the eventual clearance between the dampers and their fixing seats. In [47], experimental tests and rubber bushings optimization were presented to tune the overall dynamic stiffness of the secondary vertical dampers to avoid excessive amplifications up to 25 Hz.

In [31], the influence of a CVD SAD (shown in Fig. 12a) on the vertical car body acceleration was assessed through HIL tests, comparing SH, MPPT and LQR control logics. Figure 12b shows the improvement provided by the SH control logic, which was found to be the best control strategy among the ones considered in the research. A following work also introduced SMC to improve the robustness of the ride quality improvement and to enhance the fault tolerance of the SAD [82]. In [161], MR SADs were successfully introduced in vertical direction besides secondary coil springs to suppress car body vertical acceleration, also introducing an artificial track defect to trigger lateral bump stops. Field test results are reported in [162] implementing SAD in vertical and lateral directions, controlled according to the SH logic, improving the passengers' comfort by 25% on average.

The field tests of vertical FADs described in [116, 117] showed that the active prototypes, shown in Fig. 12e, consistently enhanced the ride quality index with respect to the passive solution along different lines, as illustrated in Fig. 12f. In particular, improved ride quality was obtained at high speeds, whilst negligible improvement was found below 120 km/h.

5.3.2 Primary vertical dampers

In 2007, Sugahara et al. [163] proposed the implementation of primary CVD SADs to mitigate the vertical car body acceleration in the frequency range of the first car body bending modes. By applying a SH controller, numerical simulations and roller rig tests confirmed a decrease in about 3 dB in the car body vertical acceleration. This concept was also tested together with SA control of air springs in field tests on the Sanyo–Shinkansen line, providing even better results [119]. More recently, Fu and Bruni [164] identified primary SADs as a promising application to improve ride quality through a wide comparative analysis considering primary and secondary SADs and FADs. A dedicated research, addressing the influence of primary SADs on the suppression of car body vertical acceleration due to modal coupling between car body bending mode and bogie pitch rotation, was proposed [165], and the results were confirmed by HIL tests considering a MR prototype [37], shown in Fig. 12c. The results obtained from HIL tests with the LQG controller are reported in Fig. 12d.

The implementation of primary FADs on a two-axle rail vehicle was proposed in [166] to mitigate the deterioration of ride quality due to bogies removal, comparing SH and LQG controllers. The analysis, which also accounted for actuator dynamics, highlighted that LQG can be more robust than SH in realistic scenarios. Giossi et al. [167] investigated a similar application for a metro vehicle, comparing FADs with modal and blended control approaches to suppress vertical car body acceleration.

5.3.3 Hydraulic interconnected suspensions (HIS)

Application of HIS at the secondary suspension stage of rail vehicles was proposed in recent years to improve the lateral comfort in terms of non-compensated lateral acceleration during curve negotiation. Active HISs were proposed to replace passive anti-roll bars to achieve a limited tilting capability [18, 168]. The interconnected layout was tested with different control logics (feed-forward + PID, feed-forward + PID with SH, LQ). Internal modal control was also integrated in a similar application [19]. The solution showed a reduction of non-compensated lateral acceleration during high-speed curving at 340 km/h, providing results similar to those of a vehicle in passive configuration running at 300 km/h.

HIS components were also implemented to mitigate vertical car body acceleration. In [169], a passive interconnected hydro-pneumatic suspension composed by a HIS in series with traditional air springs was introduced at the secondary

(a)

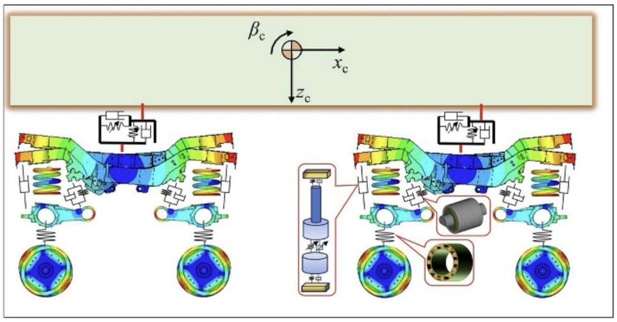

(b)

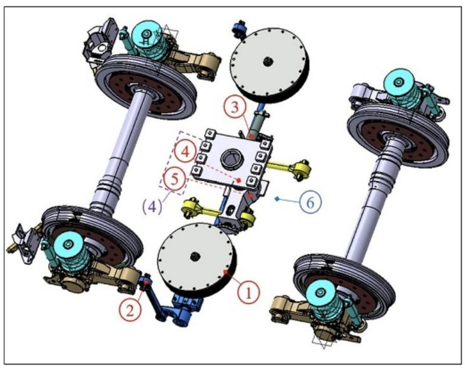

Fig. 13 **a** Schematisation of the high-frequency transmission modelling approach proposed in [89], illustrating the main transmission paths in the rail vehicle: primary coil springs, HSCs, rubber bushings, secondary springs, traction rods. **b** Secondary vibration transmission paths between bogie and car body of a metro vehicle, from [183] (the lateral damper acts in point 3)

suspension stage, achieving a reduction in the 1–3 Hz range. A passive HIS was also proposed to be implemented at the primary suspension stage to overcome the trade-off between low stiffness requirement for vibration transmission in traditional operating conditions and increased stiffness levels necessary to limit the car body roll angle in case of lateral wind gusts [20]. Secondary SA HISs were proposed by Liu et al. [93] to replace anti-roll bars. The SA layout was compared to a reference vehicle with traditional suspensions and to a passive version of the HIS, and provided better performance when excited by track unevenness and wind gusts.

5.3.4 Other components: lateral, yaw, motor and inter-car dampers

Secondary lateral and yaw dampers influence the lateral ride quality of the passengers in the rail vehicle. The sensitivity of human beings to lateral vibrations is exacerbated in the 1–3 Hz range [160, 167], a frequency range in which the car body hunting phenomenon may arise. Therefore, the HSCs already discussed in Sect. 5.1 can also directly improve ride quality by suppressing low-frequency car body vibration [170], as reported by many research works focussing on secondary lateral SADs and FADs [32, 41, 112, 171]. Shi et al. [92] focussed on the capability of lateral SADs to suppress lateral car body acceleration even at higher frequency (up to 9–12 Hz), extending the range of interest for these applications. It is also worth mentioning that FA lateral suspension aiming at improving ride quality are nowadays implemented in several in-service trains, such as Shinkansen series and the ETR1000 Italian high-speed train [152].

The correlation of yaw dampers with the high frequency transmission of vibration to the car body is less explored in the literature. The effect of the mounting layout and inclination angle was investigated using analytical [172] and numerical [173] vehicle models. Recent studies addressed the effect of yaw [174] and motor [175] damper parameters on the modal coupling between car body flexible modes and bogie hunting, highlighting that coupling between motor or bogie modes and car body bending modes can exacerbate the vibration transmission, negatively affecting ride quality.

The influence of passive longitudinal and lateral intercar dampers on ride quality was assessed by Tanifuji et al. [176], considering aerodynamic excitations. The dampers were modelled using a Kelvin–Voigt approach, and parametric analyses identified optimal stiffness and damping values to meet the trade-off between ride quality and curving performances.

5.4 High-frequency structural vibrations

Suspension components play a relevant role in the transmission of high-frequency vibration to rail vehicles components; therefore, they are correlated to bogie fatigue and interior structure-borne noise (SBN) issues.

In railway engineering, bogie fatigue issues are investigated within a frequency range up to 1000 Hz [87]. Together with primary coil springs [87, 177], the primary vertical dampers [86, 178] are relevant transmission paths for vibration, as shown in Fig. 13a. In [86], primary vertical dampers and rubber bushings were modelled using LPMs to study the vibration transmission from the wheelsets to the bogie frame. Wang et al. [87] proposed a refined modelling approach based on hybrid LPM, PM and finite element formulations to consider the primary vertical dampers and rubber bushings in the context of bogie vibration assessment.

Analyses on SBN contributions to the interior noise consider frequency ranges up to hundreds of Hz [179, 180]. Indeed, SBN is dominant over the airborne transmission path at low acoustic frequencies, especially at low speed [181]. Xiao et al. [88] investigated the influence of primary vertical dampers on the SBN contribution to interior noise. A PM was established by considering mass balance equations for compression and rebound

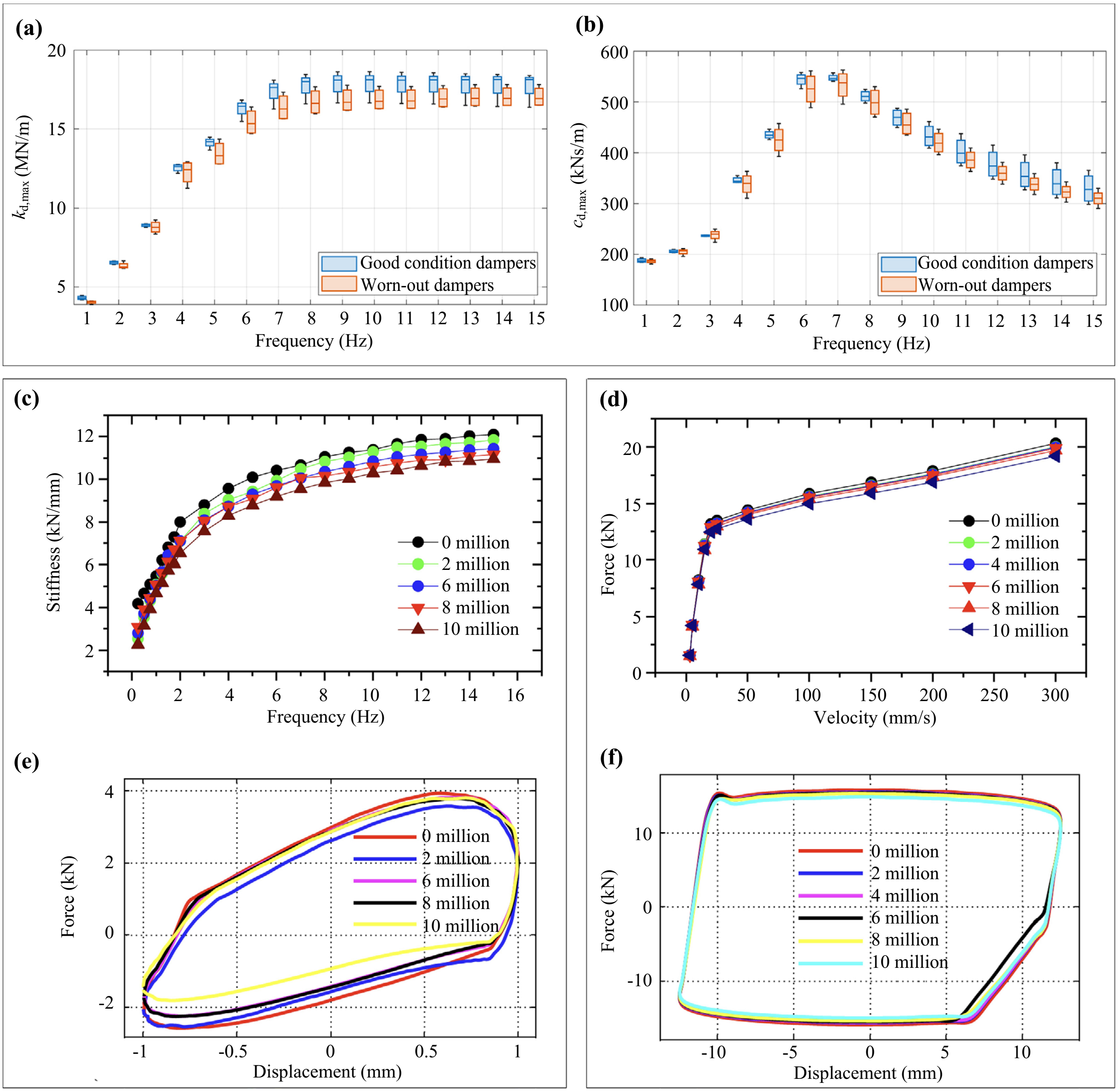

Fig. 14 Average influence of fatigue on the dynamic performance indexes of nominally equal good conditions and worn-out yaw dampers: **a** dynamic stiffness and **b** dynamic damping. From [186]: influence of intermediate service stages on **c** the dynamic stiffness of a yaw damper, obtained from **e** sinusoidal high-frequency cycles (1 mm amplitude, up to 15 Hz). **d** The static force versus velocity performance of a yaw damper at different service stages, obtained from **f** sinusoidal high-amplitude cycles (12.5 mm amplitude and 100 mm/s)

chambers, while lumped parameters were proposed to formulate the mechanical equations between damper body, piston rod, and centre pins. The contribution of the dampers was compared with the influence of rubber bushings and primary coil springs. Secondary HSCs were analysed with operational transfer path analysis to identify the most relevant transmission paths between bogies and car body. Considering a high-speed vehicle, Ström [182] experimentally identified yaw dampers as a preferential transmission path for SBN, the dominant contribution being up to 500 Hz. Preferential transmission paths through the mounting location of anti-roll bars, vertical dampers and yaw dampers proved to be relevant, especially in the one-third octave band centred at 160 Hz [181]. In metro vehicles, transmission paths through the secondary lateral damper were identified by Peng et al. [183] as relevant in the frequency range between 300 and 800 Hz. Indeed, as shown in Fig. 13b, HSCs are act as vibration transmission paths also at the secondary suspension stage, among other components such as the air springs, anti-roll bars, core plates and traction rods [183]. Moreover, experimental tests [184] correlated higher primary vertical damping to increased

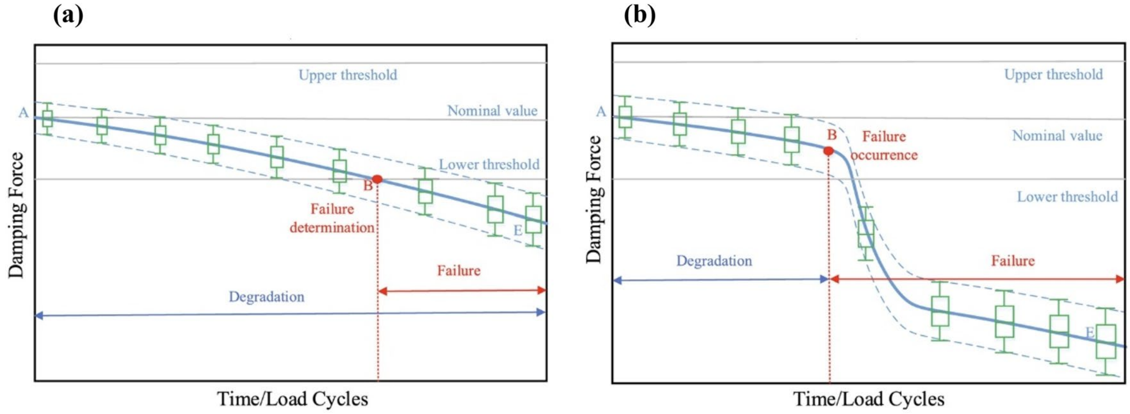

Fig. 15 Overview of the **a** experience-based failure process and **b** experience-based degradation process [186]

levels of normal floor accelerations up to 100 Hz. Secondary vertical dampers were also identified as a dominant transmission path below 250 Hz on a metro vehicle, even if in this case the SBN was dominant only below 100 Hz [185].

6 Degradation, failure and fail-safe design of hydraulic suspensions in railway engineering

According to EN 13802, the required dynamic characteristics of HSCs must be agreed upon between vehicle integrators and suspension manufacturers, and deviations in the $\pm 15\%$ range can be realistically expected [160]. Degradation and failure may affect railway HSCs during their service life, influencing the dynamic performances of the vehicle, and therefore have been the subject of intense research in recent years.

Degradation is defined as a progressive change in the performance of the component, yet remaining within acceptable limits. Degradation may introduce variations in internal sealing, the stiffness of bushings or internal components, and affects oil viscosity, eventually causing a reduction of oil volume due to leakage [186]. In the context of HSCs, degradation may result, e.g. in changes of the $k_{d,Max}$ and $c_{d,Max}$ parameters. The results obtained from four yaw dampers tested at different service life conditions (good and worn-out conditions) at Southwest Jiaotong University are reported in Fig. 14a and b. In this case, neither $k_{\mathrm{d,Max}}$ nor $c_{\mathrm{d,Max}}$ of the samples under analysis were strongly affected by degradation, even if the dynamic stiffness showed higher sensitivity.

In [186], an extensive analysis on the degradation of a yaw damper component was presented. In particular, the influence of the service mileage on the static and dynamic performance of the damper was studied by reproducing a total amount of 10 million cycles. The influence of intermediate service stages on the high frequency response of the damper can be observed from the force versus displacement cycles shown in Fig. 14e, and from the trend of the dynamic stiffness illustrated in Fig. 14c: a good correspondence with the trend reported in Fig. 14a can be observed. Moreover, the influence of the service stage on the static performance of the damper can be observed in the high amplitude force versus displacement cycles reported Fig. 14f, and summarised in the force versus velocity curves shown in Fig. 14d. Here, it can be observed that the degradation is affecting in particular the blow-off region (also known as force unloading phase [128]).

Long term degradation affects the performance of HSCs, eventually leading to excessive reduction of damping force, as illustrated in Fig. 15a. Ref. [186] investigated this phenomenon focussing on the degradation of yaw dampers' parameters with service mileage, proposing an accelerated test methodology that imposed high-amplitude high-frequency excitations able to let the damper dissipate an equivalent amount of energy with respect to the one estimated from damper displacement measurements obtained from field tests. The effects of damper degradation on force versus displacement cycles and dynamic indexes were discussed. The effect of temperature on the service life of yaw dampers was also studied in [187].

Failure can be identified as a catastrophic event leading to a severe loss of function in the HSC. As shown in Fig. 15b, the occurrence of a failure suddenly reduces the damping force, leading to insufficient energy dissipation by the device.

A comparative analysis of deterioration and failure in yaw damper components was proposed in [188]. The authors distinguished the experience-based failure process from the stochastic failure process. In experience-based failure process, a deterministic failure event can be identified (see point B in Fig. 15b): after this event, the damper provides a reduced damping force. In stochastic failure process, a threshold between acceptable and unacceptable damping force—in terms of number of load cycles—cannot be found. Therefore, inconsistent results in damping force can be obtained in a relatively large interval of load cycles, where the damper provides either acceptable or unacceptable damping force, so that the identification of the failed damper becomes more challenging in a stochastic failure process than for an experience-based failure process.

PMs can be used to investigate different failure modes of HSC, studying the variations of the suspension performances caused by the reduction of elastic bushings stiffness, the presence of series gap clearance and the amount of air dissolved in the oil [13, 73, 189]. Considering yaw damper applications, co-simulations between PMs and MB models of rail vehicles were implemented to quantify the influence of the failure modes on vehicle dynamics, identifying the detrimental effect of gap clearance on stability and ride quality [99].

PMs were also implemented to study the harmful effect of yaw dampers' empty compression strokes on vehicle dynamics [53]. This phenomenon, caused by excessive presence of air inside the oil, negatively influences bogie stability. A similar issue, exacerbated by the incorrect mounting of the damper, was also examined, suggesting the need to avoid the formation of large air quantities in the oil [81]. The effect of cavitation phenomena on vehicle stability was investigated in [190] where an extended PM considering the influence of cavitation on the force versus displacement characteristic of yaw dampers is proposed.

Failure analysis becomes even more relevant when dealing with SA and FA HSCs [191]. A comprehensive methodology for covering different active suspension failure scenarios was proposed in [192], and it was based on failure mode and effects analysis (FMEA) and fault tree analysis (FTA), considering MB simulations analysing the dynamic performance required in EN 14363 [193]. In this proposal, various failure modes were evaluated also according to their risk priority number, a function of the severity, occurrence, and detection values of each failure mode. This procedure was implemented for a case study derived from previous field tests on FA vertical dampers, where five failure modes were evaluated by quantifying the related reduction of ride quality [116]. In a similar way, a failure analysis of a CVD SA secondary vertical damper was proposed in [82], introducing artificial defects in the HIL tests of the suspension (always open or always closed valve, failure of an accelerometer). Several layouts of steering bogie based on FA HSCs were investigated in [155], and the various configurations were compared in terms of dynamic performance improvement and fault-tolerant capabilities. A fault-tolerant actuator for steering purposes was proposed in [154], characterised by a mechanical solution implemented to avoid steering forces in the opposite directions of the track, while the impact on curving performance of two failure modes was investigated in [194]: a hard failure, consisting in a stuck actuator, and a soft failure, where the actuator was not introducing any steering torque on the system.

7 Emerging trends and conclusions

This paper proposed a state-of-the-art review on the design, modelling, testing and application of HSCs, aiming to foster the development of innovative and more efficient solutions for rail vehicles with superior performance. After addressing the various topics, some emerging trends and conclusions can be identified:

- LPMs are simple and reliable models that can support the overall vehicle dynamic simulations and do not require any knowledge of the internal layout of the HSC, but they require a proper calibration based on experimental characterisation tests. Due to the limited physical meaning of the parameters, LPMs cannot accurately support predictive assessment of different HSCs layouts on the vehicle dynamics. PMs can provide superior accuracy compared to LPMs, support design optimization and failure analyses, provided that a sufficient knowledge of the internal layout of the HSC is available. DDMs are attractive in those cases when computational efficiency is a priority, but they struggle to generalise the response of HSCs under service conditions different from those considered in the training of the model; therefore, hybridization with PMs is suggested to compensate for this limitation. Future trends could explore the use of PMs for suspension layout optimization and the use of hybrid DDMs in real-time for modelling or monitoring applications.
- HIL testing is a valuable methodology to test HSCs in realistic operating conditions. This approach is a good compromise between standard characterisation tests and more complex methodologies, such as roller rig and field tests. Thanks to the possibility of varying the features of the virtual vehicle model, HIL testing can simulate various vehicle configurations, allowing the assessment of the HSC over a wide range of service conditions. In the near future, this approach could also be refined to support suspension manufacturers in the development and validation of innovative prototypes. HIL also provides a controlled environment to support failure analyses and the investigation of temperature effects, supporting the study of more robust suspensions.
- From the literature review, further research need is identified regarding testing and modelling approaches to study the effect of HSCs on the high frequency structural vibrations of rail vehicles and related fatigue and SBN issues. Also, the conclusions on the dominant transmission paths

of high frequency vibration are not fully established at present.

- While several yaw damper and lateral damper applications were proposed to improve vehicle stability, less attention was paid to the possibility of combining these devices with optimised motor and inter-car dampers. In particular, the literature search did not highlight any attempt so far to achieve the mutual optimization of yaw/motor or yaw/inter-car devices to suppress both car body and bogie hunting motions.
- Physical models of HSCs have now reached a good level of maturity and can be used to simulate many diverse defects and failures modes. This suggests the possibility of implementing PMs in Digital Twin methodologies to support the monitoring and diagnostics of HSCs. This additional feature could lead to smart HSCs having superior fault-tolerant capability and therefore enhancing the safety and reliability of rail vehicles, at the same time reducing maintenance costs.

Acknowledgements This work was supported by the National Natural Science Foundation of China (Nos. 52388102, 52272406). The first author would like to thank his wife for her continuous care and support.

References

1. Stichel S, Orlova A, Berg M (2019) Suspension elements and their characteristics. Handbook of Railway Vehicle Dynamics, 2nd edn. CRC Press, Boca Raton
2. Fu B, Hossein-Nia S, Stichel S et al (2022) Study on active wheelset steering from the perspective of wheel wear evolution. Veh Syst Dyn 60(3):906–929
3. Giossi RL, Persson R, Stichel S (2024) Wheel wear reduction of a mechatronic two-axle vehicle controlled with feedforward wheelset steering approaches. Veh Syst Dyn 62(4):1037–1062
4. Tian S, Luo X, Xiao C et al (2023) Distribution method of active steering control for rail vehicles based on overdrive characteristics. IEEE Trans Veh Technol 72(12):15634–15647
5. Hwang I-K, Hur H-M, Kim M-J et al (2018) Analysis of the active control of steering bogies for the dynamic characteristics on real track conditions. Proc Inst Mech Eng Part F J Rail Rapid Transit 232(3):722–733
6. Huang Y, Dai H, Shi H et al (2026) Influence of nonlinear motor suspension parameters on Hopf bifurcation characteristics of high-speed bogie. J Vib Control 32(7–8):1289–1302
7. Alfi S, Mazzola L, Bruni S (2008) Effect of motor connection on the critical speed of high-speed railway vehicles. Veh Syst Dyn 46(sup1):201–214
8. Wang W, Zhou Z, Zhang W et al (2020) A new nonlinear displacement-dependent parametric model of a high-speed rail pantograph hydraulic damper. Veh Syst Dyn 58(2):272–289
9. Allotta B, Pugi L, Bartolini F (2009) An active suspension system for railway pantographs: the T2006 prototype. Proc Inst Mech Eng Part F J Rail Rapid Transit 223(1):15–29
10. Polach O, Berg M, Iwnicki S (2019) Simulation of railway vehicle dynamics. Handbook of Railway Vehicle Dynamics, 2nd edn. CRC Press, Boca Raton
11. Dixon JC (2007) The Shock Absorber Handbook. Wiley, Hoboken
12. Huang C, Zeng J (2025) Innovative on-off yaw dampers with switchable dynamic stiffness for enhanced stability of high-speed railway vehicles. Proc Inst Mech Eng Part F J Rail Rapid Transit 239(4):352–370
13. Huang C, Zeng J (2018) Dynamic behaviour of a high-speed train hydraulic yaw damper. Veh Syst Dyn 56(12):1922–1944
14. Jiang C, Zhang H, Ling L et al (2023) Modelling and simulation of nonlinear dynamic characteristics of yaw dampers subjected to variable temperature operation condition of high-speed trains. Nonlinear Dyn 111(20):18931–18952
15. Alonso A, Giménez JG, Gomez E (2011) Yaw damper modelling and its influence on railway dynamic stability. Veh Syst Dyn 49(9):1367–1387
16. Gao H, Chi M, Dai L et al (2020) Mathematical modelling and computational simulation of the hydraulic damper during the orifice-working stage for railway vehicles. Math Probl Eng 2020:1830150
17. Wang WL, Yu DS, Zhou Z (2015) In-service parametric modelling a rail vehicle's axle-box hydraulic damper for high-speed transit problems. Mech Syst Signal Process 62(63):517–533
18. Di Gialleonardo E, Facchinetti A, Bruni S (2023) Control of an integrated lateral and roll suspension for a high-speed railway vehicle. Veh Syst Dyn 61(2):472–498
19. Di Gialleonardo E, Santelia M, Bruni S et al (2022) A simple active carbody roll scheme for hydraulically actuated railway vehicles using internal model control. ISA Trans 120:55–69
20. Isacchi G, Ripamonti F (2024) On the implementation of hydraulic-interconnected-suspensions at the primary suspension stage of high-speed rail vehicles. Proc Inst Mech Eng Part F J Rail Rapid Transit 238(9):1096–1107
21. Liu M, Zhang N, Zheng M et al (2026) A study of a novel hydraulically interconnected anti-hunting damping system for high-speed trains. Multibody Syst Dyn 66(1):155–180
22. Yao Y, Chen X, Li H et al (2023) Suspension parameters design for robust and adaptive lateral stability of high-speed train. Veh Syst Dyn 61(4):943–967
23. Chen X, Shen L, Hu X et al (2024) Suspension parameter optimal design to enhance stability and wheel wear in high-speed trains. Veh Syst Dyn 62(5):1230–1252
24. Song Y, Qi Y et al (2026) Multi-parameter optimization based on a surrogate model for improving vehicle dynamics and reducing wheel wear in high-speed EMUs. Veh Syst Dyn 64(2):251–274
25. Li G, Zhou Y, Yao Y et al (2023) Application of yaw dampers with frequency-selective damping to improve the locomotive adaptability to low/high conicity stability. Proc Inst Mech Eng Part F J Rail Rapid Transit 237(6):784–795

26. Isacchi G, Ripamonti F, Corsi M (2023) Innovative passive yaw damper to increase the stability and curve-taking performance of high-speed railway vehicles. Veh Syst Dyn 61(9):2273–2291
27. Lewis TD, Jiang JZ, Neild SA et al (2020) Using an inerter-based suspension to improve both passenger comfort and track wear in railway vehicles. Veh Syst Dyn 58(3):472–493
28. Zhou Y, Tian Q, Hecht M (2024) Application of hydraulic arm bushings with frequency-dependent stiffness to compromise hunting stability and curve negotiation performance for a passenger coach. J Vib Eng Technol 12(7):8839–8849
29. Goodall RM, Mei TX (2019) Active suspensions. Handbook of Railway Vehicle Dynamics, 2nd edn. CRC Press, Boca Raton
30. Isacchi G, Ripamonti F, Corsi M et al (2024) Improving curving Performances of High-speed Rail Vehicles with Semi-active Yaw Dampers. Advances in Dynamics of Vehicles on Roads and Tracks III, Springer Nature Switzerland, Cham
31. Ripamonti F, Chiarabaglio A (2019) A smart solution for improving ride comfort in high-speed railway vehicles. J Vib Control 25(13):1958–1973
32. Wu Y, Gan F, Shi H et al (2023) Experimental investigations on the semi-active control of a valve-driven secondary lateral damper for a high-speed rail vehicle. J Vib Control 29(13–14):3025–3037
33. Wang X, Liu B, Di Gialleonardo E et al (2022) Application of semi-active yaw dampers for the improvement of the stability of high-speed rail vehicles: mathematical models and numerical simulation. Veh Syst Dyn 60(8):2608–2635
34. Ahmadian M (2017) Magneto-rheological suspensions for improving ground vehicle's ride comfort, stability, and handling. Veh Syst Dyn 55(10):1618–1642
35. Wang F, Tanaka M, Nakada N et al (2004) Development of an ER bypass damper for railway car relief couplers. Int J Appl Electromagn Mech 19(1–4):269–274
36. Chonan S, Tanaka M, Naruse T et al (2004) Development of an electrorheological active buffer for railway vehicles—estimation of the capacity from prototype performance. Smart Mater Struct 13(5):1195–1202
37. Fu B, Di Gialleonardo E, Liu B et al (2024) Modelling, hardware-in-the-loop tests and numerical simulation of magneto-rheological semi-active primary suspensions in a railway vehicle. Veh Syst Dyn 62(6):1471–1494
38. Jeniš F, Michálek T, Kubík M et al (2025) Semi-active yaw dampers in locomotive running gear: new control algorithms and verification of their stabilising effect. J Vib Control 31(13–14):2538–2549
39. Oh J-S, Shin Y-J, Koo H-W et al (2016) Vibration control of a semi-active railway vehicle suspension with magneto-rheological dampers. Adv Mech Eng 8(4):1687814016643638
40. Liao Y, Liu Y, Yang S (2019) Semiactive control of high-speed railway vehicle suspension systems with magnetorheological dampers. Shock Vib 2019:5279380
41. Kim H-C, Shin Y-J, You W et al (2017) A ride quality evaluation of a semi-active railway vehicle suspension system with MR damper: railway field tests. Proc Inst Mech Eng Part F J Rail Rapid Transit 231(3):306–316
42. Guo C, Gong X, Zong L et al (2015) Twin-tube- and bypass-containing magneto-rheological damper for use in railway vehicles. Proc Inst Mech Eng Part F J Rail Rapid Transit 229(1):48–57
43. Bruni S, Vinolas J, Berg M et al (2011) Modelling of suspension components in a rail vehicle dynamics context. Veh Syst Dyn 49(7):1021–1072
44. Chen X, Yao Y, Shen L et al (2022) Multi-objective optimization of high-speed train suspension parameters for improving hunting stability. Int J Rail Transp 10(2):159–176
45. Shi H, Zeng J, Qu S (2023) Linear stability analysis of a high-speed rail vehicle concerning suspension parameters variation and active control. Veh Syst Dyn 61(11):2976–2998
46. Isacchi G, Shi H, Ripamonti et al (2025) Effect of yaw damper on different hunting motions of high-speed trains under various vehicle configurations. ICRT 2024. Shanghai, pp 535–545
47. La Paglia I, Rapino L, Ripamonti F et al (2024) Modelling and experimental characterization of secondary suspension elements for rail vehicle ride comfort simulation. Proc Inst Mech Eng Part F J Rail Rapid Transit 238(1):38–47
48. British Standards Institution (2013) Railway applications—suspension components—hydraulic dampers. BS EN 13802:2013
49. Mellado AC, Gomez E, Vinolas J (2006) Advances on railway yaw damper characterisation exposed to small displacements. Int J Heavy Veh Syst 13(4):263
50. Chen X, Zhou Y et al (2026) Improving the stability of high-speed trains using an innovative passive yaw damper. Veh Syst Dyn 64(1):226–249
51. Teng W, Shi H, Luo R et al (2019) Improved nonlinear model of a yaw damper for simulating the dynamics of a high-speed train. Proc Inst Mech Eng Part F J Rail Rapid Transit 233(7):651–665
52. Isacchi G, Corsi M, Ripamonti F (2025) Influence of yaw damper modelling on multibody simulations of rail vehicles. ICRT 2024. Shanghai, pp 476–484
53. Guo Z, Chi M, Sun J et al (2024) Experimental and numerical research on the bogie hunting of a high-speed train caused by the empty stroke of yaw damper. Veh Syst Dyn 62(7):1637–1657
54. Isacchi G, Ripamonti F, Corsi M (2023) A meta-heuristic optimization procedure for the identification of the nonlinear model parameters of hydraulic dampers based on experimental dataset of real working conditions. J Comput Nonlinear Dyn 18(9):091004
55. Ren J, Li Q, Ren Z et al (2025) Availability of five hydraulic damper models for dynamics simulation and application of two types of high-speed electrical multiple units. Int J Rail Transp 13(6):1239–1254
56. Jeniš F, Michálek T, Kubík M et al (2025) The influence of semi-actively controlled magnetorheological bogie yaw dampers on the guiding behaviour of a railway vehicle in an S-curve: Simulation and on-track test. Proc Inst Mech Eng Part F J Rail Rapid Transit 239(1):29–38
57. Bouc R (1967) Forced vibration of mechanical systems with hysteresis. In: Proceedings of the Fourth Conference on Nonlinear Oscillation. Prague, pp 315
58. Wen Y-K (1976) Method for random vibration of hysteretic systems. J Engrg Mech Div 102(2):249–263
59. Wang DH, Liao WH (2011) Magnetorheological fluid dampers: a review of parametric modelling. Smart Mater Struct 20(2):023001
60. Yang G, Spencer BF Jr, Jung H-J et al (2004) Dynamic modeling of large-scale magnetorheological damper systems for civil engineering applications. J Eng Mech 130(9):1107–1114
61. Wang DH, Liao WH (2009) Semi-active suspension systems for railway vehicles using magnetorheological dampers. Part I: system integration and modelling. Veh Syst Dyn 47(11):1305–1325
62. Zong LH, Gong XL, Xuan SH et al (2013) Semi-active H∞ control of high-speed railway vehicle suspension with magnetorheological dampers. Veh Syst Dyn 51(5):600–626
63. Fu B, Liu B, Di Gialleonardo E et al (2024) Dynamics and Control of MR Damper in Railway Vehicle Semi-active Primary Suspension. Advances in Dynamics of Vehicles on Roads and Tracks III, Springer Nature Switzerland, Cham
64. Wu Y, Zeng J, Shi H et al (2022) A hybrid damping control strategy for high-speed trains running on existing tracks. J Low Freq Noise Vib Act Control 41(3):1258–1271

65. Li Z, Ni YQ, Dai H et al (2013) Viscoelastic plastic continuous physical model of a magnetorheological damper applied in the high-speed train. Sci China Technol Sci 56(10):2433–2446
66. Bahar A, Pozo F, Meybodi MR et al (2024) Magnetorheological fluid dampers: a close look at efficient parametric models. Struct Control Health Monit 2024:6860185
67. Huang L, Zeng J, Zhou X et al (2018) Mechanical model of yaw damper and its application in the simulation of vehicle system dynamics. IOP Conf Ser: Mater Sci Eng 397:012051
68. Deng X, Zhou Y et al (2026) Modelling and application of yaw damper with frequency-selective damping on railway vehicles. Veh Syst Dyn 64(3):646–667
69. Merritt HE (1991) Hydraulic Control Systems. John Wiley & Sons, New York
70. Isacchi G, Nayir FE, Corsi M et al (2023) Hydraulic interconnected suspension for rail vehicles: a preliminary analysis. Vib Proced 50:91–97
71. Van Kasteel R, Wang CG, Qian L et al (2005) A new shock absorber model for use in vehicle dynamics studies. Veh Syst Dyn 43(9):613–631
72. Miller DS (1990) Internal flow systems. British Hydromechanics Research Association, Cranfield
73. Wang WL, Huang Y, Yang XJ et al (2011) Non-linear parametric modelling of a high-speed rail hydraulic yaw damper with series clearance and stiffness. Nonlinear Dyn 65(1):13–34
74. Mwakitabu S, Ichchou M, Bareille O et al (2024) Modelling and simulating the primary vertical hydraulic railway dampers DISPEN. J Phys: Conf Ser 2909(1):012018
75. Huang C, Ye Y, Zeng J et al (2026) Stability assessment of railway vehicles considering undefined nonlinearity in static force–velocity characteristics of hydraulic yaw dampers. Veh Syst Dyn 64(3):544–567
76. Wang WL, Zhou ZR, Yu DS et al (2017) Rail vehicle dynamic response to a nonlinear physical 'in-service' model of its secondary suspension hydraulic dampers. Mech Syst Signal Process 95:138–157
77. Wang W, Liang Y, Zhang W et al (2019) Effect of the nonlinear displacement-dependent characteristics of a hydraulic damper on high-speed rail pantograph dynamics. Nonlinear Dyn 95(4):3439–3464
78. Farjoud A, Ahmadian M, Craft M et al (2012) Nonlinear modeling and experimental characterization of hydraulic dampers: effects of shim stack and orifice parameters on damper performance. Nonlinear Dyn 67(2):1437–1456
79. Boresi AP, Chong KP, Lee JD (2010) Elasticity in engineEring Mechanics. Wiley, New York
80. Bird RB, Stewart WE, Lightfoot EN (2006) Transport Phenomena. Wiley, New York
81. Zeng P, Dai L, Chi M et al (2025) The performance failure of yaw damper caused by air entering its inner tube and its impact on hunting instability of an intercity train. Eng Fail Anal 169:109147
82. Isacchi G, Ripamonti F (2025) A robust and fail-safe semi-active vertical damper to improve ride comfort. Veh Syst Dyn 63(11):2039–2061
83. Chen X, Yao Y, Su H et al (2026) Modeling and TF-BPNN inverse modeling of a magnetorheological damper. J Vib Control, 10775463261420711
84. Tang Z, Hu Y, Qu Z (2024) Enhancing nonlinear dynamics analysis of railway vehicles with artificial intelligence: a state-of-the-art review. Nonlinear Dyn 112(17):14687–14717
85. Dai L, Chi M, Guo Z et al (2023) A physical model-neural network coupled modelling methodology of the hydraulic damper for railway vehicles. Veh Syst Dyn 61(2):616–637
86. Liu J, Jin X (2018) Research on the vibration insulation of high-speed train bogies in mid and high frequency. Shock Vib 2018:6759105
87. Wang Q, Xiao X, Han J et al (2026) Vehicle modelling for high-frequency vibration transmission through primary suspensions. Veh Syst Dyn 64(3):568–610
88. Xiao X, Wang Q, Zhang Y et al (2025) The dynamic characteristics of the hydraulic damper on the high-frequency vibration transmission of the bogie. Int J Rail Transp 13(6):1219–1238
89. Wang Q, Xiao X, Han J et al (2025) High frequency traction rod model and its structure-borne sound transmission characteristic of high-speed trains. Sci Rep 15:12940
90. Sañudo A, Nieto J, Pérez J et al (2013) High frequency modelling and validation of railway dampers. Int J Heavy Veh Syst 20(4):312
91. Bruni S, Belforte P, Cera A et al (2008) Experimental investigation of yaw damper performances: an improved and harmonised testing methodology developed within ModTrain EU project. In: the WCRR'08 International Conference, Seoul, 1–12
92. Shi H, Gan F, Zeng J (2025) Experimental investigations of valve-controlled dampers for enhanced ride comfort on high-speed rail vehicles. IEEE Trans Ind Electron 72(9):9465–9474
93. Liu M, Zhang N et al (2025) A variable stiffness anti-roll system for railway vehicles based on a hydraulic interconnection approach. Veh Syst Dyn 63(4):798–824
94. Huang C, Zeng J, Liang S (2013) Carbody hunting investigation of a high speed passenger car. J Mech Sci Technol 27(8):2283–2292
95. Xia Z, Zhou J, Gong D et al (2020) Theoretical study on the effect of the anti-yaw damper for rail vehicles. Proc Inst Mech Eng Part C J Mech Eng Sci 234(2):457–473
96. Huang C, Shi M, Zeng J (2025) Comparison of evaluation methods for the dynamic characteristics of railway hydraulic dampers. Proc Inst Mech Eng Part F J Rail Rapid Transit 239(3):290–303
97. Luo R, Teng W, Wu X et al (2020) Dynamics simulation of a high-speed railway car operating in low-temperature environments with stochastic parameters. Veh Syst Dyn 58(12):1914–1934
98. Huang C, Zeng J (2022) Comparison of the Maxwell model and a simplified physical model for a railway yaw damper in damping characteristics and vehicle stability assessment. Proc Inst Mech Eng Part F J Rail Rapid Transit 236(3):275–287
99. Wang WL, Yu DS, Huang Y et al (2014) A locomotive's dynamic response to in-service parameter variations of its hydraulic yaw damper. Nonlinear Dyn 77(4):1485–1502
100. Isacchi G, Ripamonti F, Corsi M et al (2022) A smart passive yaw damper for the reduction of lateral contact forces in low-radius curved tracks. In: WCCM-APCOM 2022. Yokohama, pp 1–10
101. Facchinetti A, Gasparetto L, Bruni S (2013) Real-time catenary models for the hardware-in-the-loop simulation of the pantograph–catenary interaction. Veh Syst Dyn 51(4):499–516
102. Gil J, Tur M, Correcher A et al (2022) Hardware-in-the-loop pantograph tests using analytical catenary models. Veh Syst Dyn 60(10):3504–3518
103. Bruni S, Bucca G, Facchinetti A et al (2025) Recent developments on pantograph-overhead line interaction. Veh Syst Dyn 63(7):1358–1394
104. Conti R, Meli E, Ridolfi A et al (2014) An innovative hardware in the loop architecture for the analysis of railway braking under degraded adhesion conditions through roller-rigs. Mechatronics 24(2):139–150
105. Allotta B, Conti R, Meli E et al (2013) Development of a HIL railway roller rig model for the traction and braking testing activities under degraded adhesion conditions. Int J Non Linear Mech 57:50–64

106. Isacchi G, Ripamonti F (2024) An experimental methodology to support development of yaw damper prototypes based on a hardware-in-the-loop test bench. Veh Syst Dyn 62(10):2614–2631
107. Yang S, Zhao Y, Liu Y et al (2023) A new semi-active control strategy on lateral suspension systems of high-speed trains and its application in HIL test rig. Veh Syst Dyn 61(5):1317–1344
108. Li H, Isacchi G, Zhang B et al (2026) Non-Hertzian wheel-rail contact modelling for real-time simulation: a case study in hardware-in-the-loop test. Int J Rail Transp 14(3):613–632
109. Wang Z, Xiao J, Zhang B et al (2024) Performance of real-time hybrid simulation for hunting dampers of high-speed trains. Struct Control Health Monit 2024:4984025
110. Watanabe N, Iida T, Umehara Y et al (2008) Development of oil damper test equipment capable of simulating the actual conditions of railway vehicles. QR RTRI 49(1):1–6
111. Zhao Y, Liu Y, Yang S et al (2022) Analysis on new semi-active control strategies to reduce lateral vibrations of high-speed trains by simulation and hardware-in-the-loop testing. Proc Inst Mech Eng Part F J Rail Rapid Transit 236(8):960–972
112. Kwak MK, Lee J-H, Yang D-H et al (2014) Hardware-in-the-loop simulation experiment for semi-active vibration control of lateral vibrations of railway vehicle by magneto-rheological fluid damper. Veh Syst Dyn 52(7):891–908
113. Shen ZY, Hedrick JK, Elkins JA (1983) A comparison of alternative creep force models for rail vehicle dynamic analysis. Veh Syst Dyn 12(1–3):79–83
114. Allen PD, Zhang W, Liang Y et al (2019) Roller rigs. Handbook of Railway Vehicle Dynamics, 2nd edn. CRC Press, Boca Raton
115. Huo W, Yue B, Liu X et al (2020) The development of stiffness-adjustable anti-yaw damper. In: Proceedings of the 26th Symposium of the International Association of Vehicle System Dynamics. Gothenburg, pp 67–71
116. Qazizadeh A, Persson R, Stichel S (2015) On-track tests of active vertical suspension on a passenger train. Veh Syst Dyn 53(6):798–811
117. Qazizadeh A, Persson R, Stichel S (2015) Preparation and execution of on-track tests with active vertical secondary suspension. Int J Railw Tech 4(1):29–46
118. Jeon C-S, Kim Y-G, Park J-H et al (2016) A study on the dynamic behavior of the Korean next-generation high-speed train. Proc Inst Mech Eng Part F J Rail Rapid Transit 230(4):1053–1065
119. Sugahara Y, Kazato A, Koganei R et al (2009) Suppression of vertical bending and rigid-body-mode vibration in railway vehicle car body by primary and secondary suspension control: Results of simulations and running tests using Shinkansen vehicle. Proc Inst Mech Eng Part F J Rail Rapid Transit 223(6):517–531
120. Li Y, Dai H, Qi Y et al (2023) Experimental study of bogie instability monitoring and suppression measures for high-speed EMUs. Proc Inst Mech Eng Part F J Rail Rapid Transit 237(10):1260–1272
121. Ye Y, Li H, Li F et al (2024) Online assessment of train hunting stability by monitoring dynamic wheel–rail displacement: why and how? Nonlinear Dyn 112(14):11993–12017
122. Sun J, Chi M, Jiao W et al (2022) Modal parameters-based hunting stability analysis of high-speed railway vehicles considering full range of equivalent conicity. Proc Inst Mech Eng Part K J Multi Body Dyn 236(3):422–439
123. Shi H, Wang J, Wu P et al (2018) Field measurements of the evolution of wheel wear and vehicle dynamics for high-speed trains. Veh Syst Dyn 56(8):1187–1206
124. Sun J, Chi M, Jin X et al (2021) Experimental and numerical study on carbody hunting of electric locomotive induced by low wheel–rail contact conicity. Veh Syst Dyn 59(2):203–223
125. Park J (2022) Investigation of low damped carbody oscillation for Korean high-speed EMU experimental train. Proc Inst Mech Eng Part F J Rail Rapid Transit 236(1):109–121
126. Guo J, Shi H, Zeng J (2024) Bifurcation and stability analysis of a high-speed rail vehicle with active yaw dampers. J Vib Control 30(15–16):3559–3571
127. Zhang H, Ran X, Wang X et al (2021) Coupling effects of yaw damper and wheel-rail contact on ride quality of railway vehicle. Shock Vib 2021:6692451
128. Li Y, Chi M, Guo Z et al (2023) An abnormal carbody swaying of intercity EMU train caused by low wheel–rail equivalent conicity and damping force unloading of yaw damper. Railw Eng Sci 31(3):252–268
129. Huang C, Dai H, Qu S (2024) Suppression of carbody hunting for a locomotive caused by low wheel–rail contact conicity by optimising yaw damper location. Veh Syst Dyn 62(9):2237–2259
130. Dong H, Zhao B, Deng Y (2018) Instability phenomenon associated with two typical high speed railway vehicles. Int J Non Linear Mech 105:130–145
131. Yan Y, Zeng J (2018) Hopf bifurcation analysis of railway bogie. Nonlinear Dyn 92(1):107–117
132. Zhang X, Li H, Cheng J et al (2023) Adaptive stability mechanism of high-speed train employing parallel inerter yaw damper. Veh Syst Dyn 61(1):38–57
133. Mao R, Zeng J, Wang Q et al (2024) Hunting stability control of high-speed bogie based on active yaw damper. J Low Freq Noise Vib Act Control 43(4):1827–1841
134. Mao R, Zeng J, Wang Q et al (2025) Simulation and experimental investigation on stability improvement for high-speed railway vehicles. J Vib Control. https://doi.org/10.1177/10775463251399574
135. Qi Y, Luo S, Zheng Y et al (2026) Stability analysis of high speed trains based on active anti-yaw damper control with electro-hydraulic actuator. Veh Syst Dyn. https://doi.org/10.1080/00423114.2026.2621043
136. Zhou J, Shen G, Zhang H et al (2008) Application of modal parameters on ride quality improvement of railway vehicles. Veh Syst Dyn 46(sup1):629–641
137. Kang W, Zeng J, Wang Q et al (2026) Self-regulating mixed damping control strategy for mitigating carbody hunting instability and vibration control in high-speed trains. Proc Inst Mech Eng Part F J Rail Rapid Transit 240(4):382–395
138. Shi H, Zeng J, Duan L (2025) Carbody swaying suppression for a high-speed rail vehicle by utilising active lateral suspension control. Veh Syst Dyn 63(10):1998–2017
139. Huang C, Zeng J, Liang S (2014) Influence of system parameters on the stability limit of the undisturbed motion of a motor bogie. Proc Inst Mech Eng Part F J Rail Rapid Transit 228(5):522–534
140. Xu K, Zeng J, Huang CH (2019) Nonlinear stability analysis of motor bogies for high-speed trains. Proc Inst Mech Eng Part F J Rail Rapid Transit 233(9):885–895
141. Wei L, Zeng J, Huang C et al (2024) Hunting stability and dynamic stress analysis of a high-speed bogie using elastic-suspended motors as dynamic vibration absorber. Veh Syst Dyn 62(9):2332–2354
142. Zhang H, Ling L, Stichel S et al (2024) Integration of bio-inspired limb-like structure damping into motor suspension of high-speed trains to enhance bogie hunting stability. Railw Eng Sci 32(3):324–343
143. Yao Y, Wu G, Sardahi Y et al (2018) Hunting stability analysis of high-speed train bogie under the frame lateral vibration active control. Veh Syst Dyn 56(2):297–318
144. Huang C, Zeng J (2024) Stability control of high-speed bogies using an adaptive vibration absorber. Proc Inst Mech Eng Part F J Rail Rapid Transit 238(6):675–691

145. Huang Y, Dai H, Huang C et al (2024) Bifurcation and Active Control of Motor Suspension to Railway Vehicle. Advances in Dynamics of Vehicles on Roads and Tracks III. Springer Nature Switzerland, Cham
146. Fujimoto H, Miyamoto M (1996) Measures to reduce the lateral vibration of the tail car in a high speed train. Proc Inst Mech Eng Part F J Rail Rapid Transit 210(2):87–93
147. Wang W, Wu Z, Liu S et al (2024) Optimisation of an inter-vehicle damper for a high-speed train. Veh Syst Dyn 62(10):2703–2728
148. Wang W, Liu S, Wu D (2023) Effect of an inter-vehicle damper on the dynamics of a high-speed train. Vib Proced 50:77–83
149. Bustos A, Rubio H, Castejon C et al (2025) Effect of the secondary suspension and intercar links on the performance of a high-speed train. Mech Mach Theory 215:106167
150. Wickens AH (2019) A history of railway vehicle dynamics. Handbook of Railway Vehicle Dynamics, 2nd edn. CRC Press, Boca Raton
151. Bruni S, Goodall R, Mei TX et al (2007) Control and monitoring for railway vehicle dynamics. Veh Syst Dyn 45(7–8):743–779
152. Fu B, Giossi RL, Persson R et al (2020) Active suspension in railway vehicles: a literature survey. Railw Eng Sci 28(1):3–35
153. Park J-H, Koh H-I, Hur H-M et al (2010) Design and analysis of an active steering bogie for urban trains. J Mech Sci Technol 24(6):1353–1362
154. Umehara Y, Kamoshita S, Ishiguri K et al (2014) Development of electro-hydraulic actuator with fail-safe function for steering system. QR RTRI 55(3):131–137
155. Fu B, Bruni S (2022) Fault-tolerant design and evaluation for a railway bogie active steering system. Veh Syst Dyn 60(3):810–834
156. Song Y, Qi Y, Liu H et al (2025) Research on the effect of electro-hydrostatic actuators (EHA) on the curve negotiation performance and wheel wear of intercity EMUs. Veh Syst Dyn. https://doi.org/10.1080/00423114.2025.2558914
157. Aizpun M, Alonso A, Vinolas J (2016) A new parameter identification methodology for the bogie rotational resistance test of a rail vehicle. Proc Inst Mech Eng Part F J Rail Rapid Transit 230(3):879–890
158. Wang K, Wen T, Sang H et al (2023) The effect of the installation angle of a high speed train yaw damper on wheel wear. Proc Inst Mech Eng Part F J Rail Rapid Transit 237(9):1152–1162
159. Kojima T, Umehara Y, Hondo T (2022) Development of active bogie steering system to improve curving performance. Q Rep RTRI 63(2):95–100
160. British Standards Institution (2024) Railway applications—ride comfort for passengers—measurement and evaluation. BS EN 12299:2024
161. Allotta B, Pugi L, Colla V et al (2011) Design and optimization of a semi-active suspension system for railway applications. J Mod Transp 19(4):223–232
162. Jeniš F, Strecker Z, Michálek T et al (2025) Ride comfort improvement of a railway vehicle by semi-active damping control–field tests. Veh Syst Dyn. https://doi.org/10.1080/00423114.2025.2598019
163. Sugahara Y, Takigami T, Sampei M (2007) Suppressing vertical vibration in railway vehicles through primary suspension damping force control. J Syst Des Dyn 1(2):224–235
164. Fu B, Bruni S (2022) An examination of alternative schemes for active and semi-active control of vertical car-body vibration to improve ride comfort. Proc Inst Mech Eng Part F J Rail Rapid Transit 236(4):386–405
165. Fu B, Liu B, Di Gialleonardo E et al (2023) Semi-active control of primary suspensions to improve ride quality in a high-speed railway vehicle. Veh Syst Dyn 61(10):2664–2688
166. Pacchioni A, Goodall RM, Bruni S (2010) Active suspension for a two-axle railway vehicle. Veh Syst Dyn 48(sup1):105–120
167. Giossi RL, Shipsha A, Persson R et al (2022) Towards the realization of an innovative rail vehicle—active ride comfort control. Control Eng Pract 129:105346
168. Colombo EF, Di Gialleonardo E, Facchinetti A et al (2014) Active carbody roll control in railway vehicles using hydraulic actuation. Control Eng Pract 31:24–34
169. Luo R, Liu C, Shi H (2022) Dynamic simulation of a high-speed train with interconnected hydro-pneumatic secondary suspension. Proc Inst Mech Eng Part F J Rail Rapid Transit 236(5):570–581
170. Pan W, Sun J, Chen X et al (2026) Research on dynamic interaction between seated human and railway vehicle focusing on carbody swaying. J Vib Control. https://doi.org/10.1177/10775463251413120
171. Orvnäs A, Stichel S, Persson R (2011) Active lateral secondary suspension with $H\infty$ control to improve ride comfort: simulations on a full-scale model. Veh Syst Dyn 49(9):1409–1422
172. Dumitriu M, Stănică DI (2020) Effect of the anti-yaw damper on carbody vertical vibration and ride comfort of railway vehicle. Appl Sci 10(22):8167
173. Isacchi G, Corsi M, Ripamonti F (2023) Ride comfort assessment of high-speed rail vehicles: influence of yaw dampers installation angle. Vib Proced 50:98–104
174. Zhang H, Li R, Ling L et al (2025) Dynamic analysis for the carbody chattering phenomenon induced by hunting instability of high-speed train. Nonlinear Dyn 113(14):17903–17932
175. Huang C, Zeng J (2022) Suppression of the flexible carbody resonance due to bogie instability by using a DVA suspended on the bogie frame. Veh Syst Dyn 60(9):3051–3070
176. Tanifuji K, Sakanoue K, Kikko S (2008) Modelling of aerodynamic force acting on high speed train in tunnel and a measure to improve the riding comfort utilising restriction between cars. Veh Syst Dyn 46(sup1):1065–1075
177. Liu X, Thompson D, Squicciarini G et al (2021) Measurements and modelling of dynamic stiffness of a railway vehicle primary suspension element and its use in a structure-borne noise transmission model. Appl Acoust 182:108232
178. Li F, Qin H, Ma X et al (2025) In-situ testing method for high-frequency vibration transmissibility of railway vehicles. Measurement 256:117993
179. Thompson D (2024) Vehicle interior noise. Railway Noise and Vibration. Elsevier, Amsterdam
180. Zhang J, Xiao X, Sheng X et al (2020) An acoustic design procedure for controlling interior noise of high-speed trains. Appl Acoust 168:107419
181. Li M, Zhu Z, Deng T et al (2021) An investigation into high-speed train interior noise with operational transfer path analysis method. Railw Eng Sci 29(1):1–14
182. Ström R (2014) Operational transfer path analysis of components of a high speed train bogie. Dissertation, Chalmers University of Technology
183. Peng L, Han J, Nie J et al (2022) Transfer path contribution to floor vibration of metro vehicles based on operational transfer path analysis method. Chin J Mech Eng 35:23
184. Wang J, Ding X, Liu Z et al (2023) An experimental study on abnormal vibration of metro trains caused by out-of-round wheels. Proc Inst Mech Eng Part F J Rail Rapid Transit 237(2):224–231
185. Zhang Y, Li L, Zhou J et al (2025) Contributions separation prediction for multi-dimensional vibration transmission in the bogie system to metro interior noise. J Vib Control. https://doi.org/10.1177/10775463251412209

186. Dai L, Li Y, Chi M et al (2024) Accelerated degradation test method and performance prediction with service mileage of the yaw damper in railway vehicles. Eng Fail Anal 161:108285
187. Hu Z, Song D, Zeng Y et al (2021) Analysis of the service life of railway hydraulic dampers considering temperature and loading. Proc Inst Mech Eng Part F J Rail Rapid Transit 235(1):3–11
188. Zeng Y, Song D, Zhang W et al (2021) Stochastic failure process of railway vehicle dampers and the effects on suspension and vehicle dynamics. Veh Syst Dyn 59(5):703–718
189. Wang W, Yu D, Xu R (2017) Prediction of the in-service performance of a railway hydraulic damper. Proc Inst Mech Eng Part F J Rail Rapid Transit 231(1):19–32
190. Gao H, Sun J, Shiju E et al (2024) Cavitation induced hydraulic yaw damper failure and its effect on railway vehicle dynamic stability. Eng Fail Anal 161:108318
191. Mei TX, Goodall RM (2003) Recent development in active steering of railway vehicles. Veh Syst Dyn 39(6):415–436
192. Qazizadeh A, Stichel S, Persson R (2018) Proposal for systematic studies of active suspension failures in rail vehicles. Proc Inst Mech Eng Part F J Rail Rapid Transit 232(1):199–213
193. British Standards Institution (2022) Railway applications—testing and simulation for the acceptance of running characteristics of railway vehicles—running behaviour and stationary tests. BS EN 14363:2016+A2:2022
194. Mirzapour M, Mei TX, Jin X (2014) Fault detection and isolation for an active wheelset control system. Veh Syst Dyn 52(sup1):157–171